Distinguishing diapirs from inflated plutons:

Mccarthy, W.; Petronis, M. S.; Reavy, R. J.; Stevenson, C. T.

DOI:
10.1144/jgs2014-067

Document Version
Peer reviewed version

Citation for published version (Harvard):
Mccarthy, W, Petronis, MS, Reavy, RJ & Stevenson, CT 2015, 'Distinguishing diapirs from inflated plutons: an integrated rock magnetic fabric and structural study on the Roundstone Pluton, western Ireland', *Geological Society. Journal*, pp. 2014-067. https://doi.org/10.1144/jgs2014-067

Title

Distinguishing diapirs from inflated plutons: an integrated rock magnetic fabric and structural study on the Roundstone Pluton, western Ireland.

Authors and Affiliations

[1*] William McCarthy; [2]Michael S. Petronis; [3] R. John Reavy; [4]Carl T. Stevenson

1. Department of Earth & Environmental Sciences, University of St Andrews, St Andrews, Fife, KY16 9AL, UK
2. Environmental Geology, Natural Resource Management Department, New Mexico Highlands University, Las Vegas, NM 87701, USA.
3. Geology, School of Biological Earth and Environmental Sciences, University College Cork, Cork, Ireland.
4. School of Geography, Earth and Environmental Sciences, University of Birmingham, Birmingham, B15 2TT, UK.

* Corresponding author: (wmccarthy@nmhu.edu)

Abstract: Granitoid plutons account for much of the continental crust and are critical in the generation of several economic resources. Despite over a century of research, the fundamental process by which large felsic bodies intrude remains controversial. Two contrasting models persist: 1) mass ascent and subsequent cooling of magma (diapirism) and 2) sheet ascent and subsequent emplacement (laccoliths). The latter hypothesis is different from the former as distinct ascent and emplacement processes must occur and be identifiable; traditional field methods rarely allow this important distinction to be made.

We present field, petrographic and Anisotropy of Magnetic Susceptibility data from the Roundstone Pluton, Connemara, western Ireland. Previously considered a diapiric intrusion, these new data reveal anomalous sub-vertical magmatic lineations in the core of this circular intrusion as well as a suite of magmatic and submagmatic fabrics that parallel NNW-SSE country rock faults and coeval G2 sheets within the pluton. We deduce that these structures reflect a distinct centralised ascent process along a NNW-SSE conduit. Lateral emplacement and pluton inflation followed, ultimately forming a punched laccolith. We conclude that the combined application of the above techniques provides a unique insight into pluton architecture that removes ambiguity between sharply contrasting diapiric and inflated pluton models.

Supplementary material: Complete rock magnetic data tables and sample site co-ordinates (Irish Grid) are available at www.geolsoc.org.uk/SUP0000.

1 Introduction

The emplacement of large igneous bodies (with particular reference to granitoid compositions) in the crust is a fundamental process throughout the evolution of the Earth and a major control in the distribution of critical resources such as geothermal energy sources and mineral deposits. Fundamental to this significant topic is the debate about how large volumes of magma transit and are accommodated in the crust (e.g. Miller & Paterson (1999), Petford & Clemens (2000), He *et al.* (2009) and Petronis *et al.* (2012)). However, despite more than a century of research (e.g. Gilbert (1877), Clough *et al.* (1909), Harker (1909), Marzec (1927), Richey (1927), Pitcher (1977), Pitcher (1979), Marsh (1982), Corry (1988), Ramsay (1989), Weinberg & Podladchikov (1994), Vigneresse & Clemens (2000), Petford *et al.* (2000), Burov *et al.* (2003), Coleman *et al.* (2004), Vigneresse (2004), Stevenson *et al.* (2006) Forien Carlo (2009) and Magee (2012)), there remains a lack of consensus on the fundamental mechanism of pluton and batholith construction. Two end-member models regarding the transport of magma through the crust persist: 1) a singular diapiric mass migrates upwards through the crust (Marzec 1927, Ramberg 1970) or 2) batches of magma ascend along discrete sub-vertical conduits and subsequently amalgamate and are emplaced as an inclined or sub-horizontal tabular body guided by pre-existing structures in the Earth's crust (Gilbert 1877, Daly 1933, Corry 1988). The second scenario makes a clear distinction between ascent and emplacement (Jacques & Reavy 1994) by insisting that ascent is magma transport from the source region to the emplacement level only; this could occur as a series of discrete magma batches or sheets which are transported to some level in the crust, commonly within major deep-seated crustal lineaments and shear zones (Hutton 1990, Jacques & Reavy 1994, Petronis *et al.* 2012, Hutton & Reavy 1992). Emplacement then is a process exclusive to the arrival level, commonly as inflated balloons and laccoliths or as sub-horizontal inflated tabular sheets. Diapiric models do not distinguish between magma ascent and emplacement as a crystallized diapir essentially reflects the geometry of the body as it ascended.

A major problem impeding our ability to resolve the current debate is that field evidence to support either process can be frustratingly equivocal. Field evidence used to support diapiric models are summarized by Hutton (1996), these include: (1) crude concentric facies zonation, (2) an internal concentric foliation pattern which increases in intensity near contact margins, (3) shortening of host strata perpendicular to pluton contacts and (4) non-coaxial shear sense indicators that preferentially indicate diapiric growth.

These criteria have been used to interpret plutons as diapirs across a broad spectrum of geological settings (e.g. Paterson *et al.* (1989), England (1990), Vernon and Paterson (1993), He *et al.* (2009)). However, none of these characteristics are exclusive to the diapiric model, in fact all equally support models which cite magma ascent, as defined above, and subsequent inflation/ballooning of magma to form inflated laccoliths. Accordingly, several models depict the forceful growth of tabular laccoliths following a distinct ascent process (Hutton 1988, Hutton & Reavy 1992, Vauchez *et al.* 1997, Clough *et al.* 1909, Richey 1927, Anderson 1936, Stevenson 2008, O'Driscoll *et al.* 2006, Petronis *et al.* 2012, Magee *et al.* 2012). Johnson *et al.* (2003) show that field relationships alone provide insufficient evidence to distinguish between these contrasting emplacement mechanisms.

The Ardara Pluton in Donegal, north-western Ireland (Pitcher & Berger 1972, Holder 1979) illustrates this ambiguity. In this instance, concentric foliations and facies distribution have been used to support a laccolith ballooning model (Pitcher & Berger 1972, Molyneux & Hutton 2000, Hutton & Siegesmund 2001) but also a nested diapir model (Vernon & Paterson 1993). In fact, a multitude of studies report rather similar field relationships but argue for contrary emplacement models, these include the Birch Creek Pluton (Nelson & G 1971), the Papoose Flat Pluton (Morgan *et al.* 1998), the Cannibal Creek Pluton (Bateman 1985), the Criffel Pluton (Courrioux 1987), the Flamanville Granite (Brun *et al.* 1990), and the Fangshan Pluton (He *et al.* 2009). In all of these examples, much of the field data available are not exclusively supportive of either diapiric or laccolithic models. Most often, this problem arises due to a lack of detailed structural data from the interior of the pluton which often exhibits subtle fabrics or appear visually isotropic. However, it has been known for some time that granitoid bodies are not isotropic and subtle fabrics can be detected through the use of detailed rock magnetic studies (Bouchez 1997, Tarling & Hrouda 1993, Borradaile & Jackson 2010).

To unequivocally determine which of the two conflicting models is operating, a way must be found to demonstrate that some fabrics within a pluton can be exclusively attributed to a distinct ascent process and not emplacement. For example, anomalous magmatic sub-vertical linear fabrics at the centre of a pluton may indicate a central ascent site. If such features can be identified, emplacement can then be recognized as a distinct separate process and diapirism is untenable.

The Roundstone Pluton constitutes part of the late Caledonian Galway Granite Complex (McCarthy 2013) that intrudes intensely folded Argyll Group metasediments, of the Dalradian Supergroup, and Ordovician Orthogneisses in Connemara, County Galway, western Ireland (Fig. 1) (Leake & Tanner 1994). This intrusion was first described as an essentially homogenous circular shaped granodiorite that

exhibits a weak to moderate marginal concentric foliation and lacks significant internal fabrics (Leake 1969). In the absence of more detailed information on the internal architecture of the pluton, and in a similar manner to the examples discussed above, Leake (2011) concludes that this is a forcefully emplaced diapir.

Figure 1

In this contribution we present new field, rock magnetic and petrographic data from the Roundstone Pluton and the structure of the surrounding host rock. These new data facilitate a reassessment of the internal architecture of this intrusion and allow the development of a more sophisticated and detailed emplacement model. We demonstrate that the circular shaped Roundstone Pluton is a composite of two granodiorite facies with a complex internal architecture that was not previously recognized by traditional field methods. Our data show a strong geometric relationship between fabrics detected in the core of the pluton and NNW-SSE faults in the host rock that predate magmatism (Leake & Tanner 1994). Magma ascent was achieved along central concurrently active NNW-SSE shear zones and initial lateral emplacement was succeeded by a phase of inflation and vertical thickening to eventually form a punched laccolith (Corry 1988). We conclude that attainment of high resolution AMS data, utilized in conjunction with detailed field and petrographic structural data, offers a new and unique insight into the mechanisms of pluton construction, especially in cases where ambiguity follows visually isotropic pluton interiors.

2 Geological Setting

Reconnaissance mapping by the Geological Survey of Ireland (Kinahan 1869, Kinahan 1878) identified the Roundstone Pluton as a slightly oval shaped, single facies, granodiorite body (7.5 km x 8 km elongate along ~ N-S axis) that intrudes a suite of highly deformed metamorphic rocks (Fig. 2), i.e. the Connemara Metamorphic Complex (Leake & Tanner 1994). The Connemara Metamorphic Complex is understood to have been thrust southwards over the underlying Delaney Dome Formation along the Mannin Thrust (Leake *et al.* 1983) between ~468-450Ma prior to the intrusion of the Roundstone Pluton (Leake & Leggo 1963, Harvey 1967, Leake 1969, Leake & Singh 1986, Leake *et al.* 1984). A suite of conjugate northwest-southeast and northeast-southwest strike-slip faults (D5) cross cut the Connemara Metamorphic Complex and abut against, and rarely offset, the margins of the Roundstone Pluton (Leake & Tanner 1994).

Figure 2

The granodioritic Roundstone Pluton is understood to be one of the earliest members of the Galway Granite Complex (Feely *et al.* 2010, McCarthy 2013). Pluton contacts are described as variably stoped and faulted in the south, east and north while in the southwest an intrusive contact is exposed between the Roundstone Pluton and the Carna Pluton. Leake (1969) describes a weak marginal contact-parallel foliation, the rare occurrence of stoped blocks within the intrusion and several peripheral granite sheets within the immediate host rock (Fig. 2). Leake (2011) draws on these features as evidence for emplacement by upwards movement of magma driven by density contrast, i.e. diapirsim.

3 Field Relationships

The host rocks to the Roundstone Pluton and its margins have been described in detailed by several authors (see Leake and Tanner (1994) and references therein). Here, new observations are incorporated with these earlier works with an emphasis placed on their relevance to the internal architecture of the intrusion.

The attitude of the host rock foliation at the contact of the Roundstone Pluton varies from highly oblique to contact parallel (Fig. 2). To the north, the pluton cross cuts a series of D3 ESE-WNW trending asymmetrical near isoclinal folds within the Dalradian host strata (Leake 1969, Evans & Leake 1970). The western and south-eastern margin is in direct contact with Ordovician metagabbros and orthogneisses of the Connemara Metamorphic Complex (Morton 1964, Harvey 1967, Benjamin 1968, Friedrich *et al.* 1999b, Friedrich *et al.* 1999a). Exposed pluton contacts are defined by stoped or sub-vertical - steeply outward dipping faults. This is best observed on Lehanagh South Peninsula (079685, 240648) where the schistose host rock foliation (~110 - 80°N) is truncated, without significant distortion, by the sub-vertical easterly dipping faulted pluton contact. Deformation of the country rock is limited to within 50m of the contact and is defined by progressively intensive brecciation as the contact is approached. In the granite, faulted contacts are most often defined by moderate contact parallel foliations up to 100m of the country rock and a protocataclastic texture of brecciated, hydrothermally altered granodiorite that is cross cut by 5-40mm stockwork quartz veins within 20m of the contact. Sub-vertical, sharp, unchilled stoped contacts are most often observed in the east. These comprise angular or sub-angular fragments of local country rock xenoliths that are suspended in or are partially enveloped by intruding magma. Sheets associated with stoping rarely extend for more than 100m (Evans & Leake 1970) and within the pluton stoped block xenoliths are very rare (see Leake (2011)).

There is no obvious relationship between inherent host rock structure and the observed shape of the Roundstone Pluton. Sub-vertical faulted contacts, stoped contacts and peripheral granodiorite sheets emanating from the pluton define a near perfect circular outline in map view that cross cut the prominent WNW-ESE country rock foliations and folds. Thus, the field relationships show this to be a discordant pluton with minimal distortion to the host rock.

3.1 Facies Distribution and Fabric Development

The Roundstone Pluton was previously interpreted as an essentially homogenous granodiorite body with one minor sub-facies mapped in the northwest corner of the pluton (Leake 1969). The current work demonstrates that the Roundstone Pluton is in fact composed of two granodiorite facies, G1 and G2, which are mineralogically and texturally distinct.

G1 forms the outer portion and majority of the intrusion while G2 occurs as an extensive network of sheets that cross cut G1 in the core of the intrusion (Fig. 2). G1 is a phanerocrystalline (~15mm) equigranular biotite, hornblende granodiorite (2-5mm) with euhedral to subhedral plagioclase and K-feldspar. Averaged rock mode is: 46.6% plagioclase, 23.4% quartz, 21% alkali feldspar, 7% biotite, 1% hornblende and 1% accessory titanite, apatite, magnetite, rutile and zircon. Orthoclase, the predominant alkali feldspar, contains obvious micro-perthitic intergrowths and larger phenocrysts often contain numerous inclusions of quartz, feldspar and biotite (Fig. 3a). Plagioclase is sometimes strongly zoned, giving rise to selectively seritised calcic-rich cores. Leake (1969) described a quartz rich orthoclase poor finer grained subfacies of G1 (G1a) along the northeast margin of the intrusion which shares a gradational contact with G1 (Fig. 2).

G2 is typically a fine grained (0.5-2mm) equigranular biotite granodiorite which contains characteristic 3-5mm xenocrysts of strongly zoned plagioclase feldspar and rounded quartz (Fig. 3b). Averaged rock mode is; 41.6% plagioclase, 39.4% quartz, 13.3% alkali feldspar, 5% biotite and trace epidote, hornblende, magnetite, zircon and rutile. Thus, G2 sits on the opposite side of the granodiorite field adjacent to the tonalite field while G1, having a greater proportion of K-feldspar and less quartz, represents a granodiorite approaching the monzogranite field. Rounded quartz and strongly zoned plagioclase feldspar porphyritic xenocrysts (Fig. 3b) are distinctive characteristics of G2 that are interpreted as reflecting a more dynamic mixing history in G2 relative to G1.

In both facies, magnetite exhibits moderate grain boundary and fracture surface maghemitization and is spatially associated with fresh-partially chloritised biotite (Fig. 3c). Individual magnetite grains are typically included within and aligned parallel to biotite cleavage planes (Fig. 3c). Interstitial magnetite nucleates along silicate crystal lattices or is randomly orientated within the groundmass.

G2 occurs as a plexus of sheets that intrude G1 in the centre of this pluton. These intrusions dominantly strike NNW-SSE and lie parallel to earlier D5 host rock faults and late porphyritic dykes noted by Leake (1969) and Evans and Leake (1970). Poor exposure hampers efforts to map the inner part of the Roundstone Pluton in detail however a plot of the spatial occurrence of G2 outcrops reveals an overall distribution along a NNW-SSE axis across the intrusion's core (Fig. 2). These vertical and sub-horizontal metre scale G2 sheets cross cut G1, contacts are sharp, lobate or diffuse and coeval inclusions of G2 are observed in G1 (Fig. 3d). Together, these observations show the near coeval nature of G1 and G2 and indicate that pre-existing NNW-SSE D5 faults likely controlled ascent of G2 magma.

Figure 3

Fabric Development

A sub-vertical weak-moderate concentric marginal foliation, defined by 3-6mm elongate quartz ribbons (axial ration ~ 1:3) and aligned biotite (Fig. 3e), occurs within 100m of the Roundstone Pluton contact. In thin section, ribboned quartz is extensively recrystallised via bulging and biotite shows minor kinks and smearing. Larger feldspars are brecciated or show marginal recrystallisation, weak undulose extinction, brittle fractures are infilled with primary quartz & feldspar which themselves exhibit weak grain scale plastic deformation. Collectively, these data indicate fabric development occurred in the low temperature sub-magmatic state (Bouchez *et al.* 1992, Hirth & Tullis 1992, Vernon 2004, Passchier 2005).

This study identifies a second distinct zone of strain that is expressed as a weak, broadly contact parallel, sub-vertical foliation zone 1km wide ~1-2 km from the pluton's external contact. This subtle fabric is most intense in the east and west and is defined by weakly aligned euhedral feldspars and biotite as well as elongate quartz exhibiting an axial ratio ~ 2:1 (Fig. 3f). Traversing to the north and south fabric intensity diminishes completely. Significantly, the inner strain zone is micro-structurally distinct from the outer pure shear fabric discussed above in that quartz shows extensive recrystallisation by sub-grain boundary rotation and quartz ribbons wrap around partially aligned euhedral feldspars. Euhedral biotite is aligned parallel to the primary foliation and limited wedged twinning is observed in plagioclase. These observations are consistent with fabric development in the high temperature sub-magmatic state.

3.3 Summary of Field Data

The Roundstone Pluton is composed of two main facies, G1 forms the majority of the intrusion and G2 occurs as a plexus of steeply inclined NNW-SSE striking sheets that cross cut G1 along the core of the intrusion. Lobate and gradational contacts between G1 and G2 coupled with a complete lack of chilled margins unequivocally demonstrate that these facies intruded in close succession. Concentric foliations around the periphery of the intrusion exhibit low temperature sub-magmatic microstructures. The attitude and nature of these foliations are consistent with a progressive inflation and ballooning model similar to that proposed for the Ardara Pluton, Donegal (Molyneux & Hutton 2000, Hutton & Siegesmund 2001). However, owing to their subtle nature and lack of marginal syn-magmatic shear sense indicators, the current data set does not preclude other models such as the diapiric model, also suggested for the Ardara Pluton (Vernon & Paterson 1993, Paterson *et al.* 1995). Adding further complexity to the issue is the presence of the elliptical inner strain zone which strikes NNW-SSE parallel to G2 sheets and prominent D5 country rock faults.

AMS data presented here allows for the distribution of strain to be mapped in unprecedented detail allowing a clear interpretation of the emplacement of the Roundstone Pluton in the context of the above field data.

4 Rock Magnetic Investigation

4.1 Field Methods

In total, 177 orientated block samples were collected from the Roundstone Pluton along an evenly distributed grid with 100-300m intervals between sample sites. On average, 15 21mm x 25mm cylindrical sub-specimens were taken from each sample block using a non-magnetic abrasive diamond tip drill bit following the parameters set by Owens (1994). Sub-specimens from all 177 blocks underwent AMS analysis. Several representative specimens from each facies were selected for detailed rock magnetic experiments to determine the dominant magnetic mineralogy of both facies and to identify or eliminate the possible presence of complicating features (e.g. Potter and Stephenson (1988), Rochette (1988), Wolff *et al.* (1989), Hargraves *et al.* (1991), Stephenson (1994), Cañón-Tapia (1996), Cañón-Tapia (2001), Aubourg and Robion (2002), Bouchez *et al.* (2006), Gaillot *et al.* (2006), Chadima *et al.* (2009), Almqvist *et al.* (2010) and Fanjat *et al.* (2012)).

4.2 Results of Rock Magnetic Experiments

Results of standardized rock magnetic experiments from six representative sample sites, four from G1 (RD15, RD25, RD32, RD99) and two from G2 (RD108, RD122), are presented below. In addition, the thermal demagnetization behaviour of three component IRM (modified from Lowrie (1990)) from two samples (RD25 and RD122) is presented to better constrain the principal ferromagnetic contributors to the AMS tensor. All experiments were carried out in the New Mexico Highlands University Palaeomagnetic Lab. Summary diagrams for all rock magnetic experiment results are presented in Figure 4.

Figure 4.

Temperature dependence of susceptibility

Curie Point estimates (T_C) were determined by measuring continuous low field susceptibility during stepwise heating and cooling of powdered samples between room temperature and 700°C in an argon saturated atmosphere (Fig. 4a). Six out of seven samples exhibit a well defined peak in susceptibility which, using either the inflection point or the Hopkinson Peak methods (Hopkinson 1890, Moskowitz 1981, Tauxe 1998) return estimated T_C values between 575°C - 580°C. Using T_C as a proxy for Ti content in magnetite (Akimoto 1962, Lattard *et al.* 2006), these data indicate a dominance of near stoichiometric magnetite (Ti < 0.1%) in the majority of samples. Distinctive Hopkinson Peaks, consistent with the presence of single domain magnetite (Orlický 1990), were not detected. All specimens are irreversible on the cooling curve and show a net increase in bulk susceptibility between 10-25% (failing RD25 which increased by 100%). Distinct increases in bulk susceptibility that occur between 270-340°C on several heating curves (e.g. Fig. 4a, RD122 & RD32) are absent on respective cooling curves. This feature is consistent with the presence of titanomaghemite but may also indicate the presence of iron sulphides, such as pyrrhotite, and are discussed below in light of other petrographic and magnetic data.

Low temperature susceptibility experiments from -197°C to 10°C (room temperature) is a useful means of determining the relative contribution of paramagnetic and ferromagnetic phases to bulk susceptibility & the AMS tensor (Martín-Hernández & Hirt 2001, Richter & Pluijm 1994). Ideal ferromagnetic curves show initial abrupt increases in susceptibility followed by an essentially flat line (little subsequent temperature dependence) while ideal paramagnetic curves show steady decreases in bulk susceptibility during heating (i.e. a line described by the Curie-Weiss Law) (Richter & Pluijm 1994). Here, results show good correlation between all samples with initial rapid increases in susceptibility between -197°C and -

175°C followed by a subsequent gradual temperature dependence in bulk susceptibility (Fig. 4b). This data is consistent with the presence of magnetite, shown by the abrupt increase and plateau in susceptibility pre and post -175°C, and minor paramagnetic phases, which cause the observed negative temperature dependence below -175°C. This experiment shows that paramagnetic phases have a negligible, and magnetite an overwhelmingly dominant, contribution to bulk susceptibility at room temperature.

IRM acquisition and BIRM

Measuring the acquisition of saturation isothermal remnant magnetization (IRM) and back-field isothermal remnant magnetization (BIRM) aids in determining magnetic mineralogy and grain size (Dunlop & Özden 1997, Dunlop 1972). IRM acquisition curves (Fig. 4d) show a rapid increase in remanence in low inducing fields that reach 95% saturation between 0.13 - 0.25T, complete saturation (M_S) is always reached prior to 0.4T. No significant increase is noted between 0.4T and 2.5T. The coercivity of remanence (H_{CR}), extrapolated from BIRM curves (Fig. 4c), is reached in fields between 0.035 - 0.062T for all samples. Results of BIRM and IRM experiments are consistent in that samples requiring higher saturating fields also require higher BIRM fields to reach H_{CR}.

Lowrie - Fuller Test

A modified Lowrie - Fuller Test (Lowrie & Fuller 1971) was carried out to constrain the coercivity parameters of constituent minerals in each sample (Fig. 4e). NRM demagnetization curves gently undulate reflecting stripping of increasingly stable NRM and typically have median destructive field (MDF) values of <20mT. ARM and SIRM demagnetization curves have MDF values between 7-19mT and are fully demagnetization (≤95%) in fields of ≤125mT.

A negligible distinction between the stability of ARM and SIRM demagnetization curves (a difference of <4mT) is noted and thus the Lowrie - Fuller test, in itself, is inconclusive (Dunlop *et al.* 1973, Bailey & Dunlop 1983, Heider *et al.* 1992, Xu & Dunlop 1995). Here, curve profiles and ARM median destructive field values of >20mT are used as a proxy for grain size and thus domain state (Argyle & Dunlop 1990). These data suggests all specimens are dominated by MD magnetite with a minor component of slightly higher coercivity PSD magnetite influencing RD32, RD108 and RD15.

Three-Component IRM Demagnetization

The above results are consistent with the dominance of coarse grained low Ti magnetite in the studied samples, subtle variations in magnetic mineralogy do occur and the presence of titanomaghemite (as

distinct from maghemite, the fully oxidized en-member of pure magnetite) or iron sulphides is indicated. A three-component IRM demagnetization test (modified after Lowrie (1990)) is used here to determine the relative contribution made to magnetic remanence by ferromagnetic phases within specified coercivity spectra in two specimens (RD25, RD122). Inducing fields of 0.03, 0.3T and 3.0T were selected and results are illustrated in Figure 4f.

The modulus demagnetization curve shows that both samples demagnetized rapidly between 0-300°C and at a more stable rate between 300-700°C, inspection of the three orthogonal components of the composite IRM (0.03T, 0.3T and 3.0T component vectors) show similar demagnetization patterns. Analysis of the 0.3T component shows intermediate coercivity phases are dominant and present in comparable proportions in both samples. Although the 0.3T component decays rapidly between 0-300°C full demagnetization is not achieved until ~580°C. This is consistent with the presence of two separate magnetic phases, one with a lower unblocking temperature (probably MD titanomaghemite or pyrrhotite) and a second with a higher unblocking temperature (most likely MD-PSD magnetite). The soft fraction (0.03T) component is most abundant in RD25, and demagnetizes continuously to ~580°C, and a minor contributor in RD122 where it is fully demagnetized by 400°C. We interpret these profiles as magnetically soft, coarse grained, magnetite and titanomaghemite respectively. The 3.0T component contributes equally to remanence in both samples and demagnetizes in comparable fashion, i.e. rapidly between 0-300°C and at a declined rate between 300°C up to 650°C. Both pyrrhotite and hematite have magnetic saturation values higher than stoichiometric magnetite and respective T_C values of ≤320°C and ≤675°C respectively (O'Reilly 1984, Clark 1984, Dekkers 1988).

4.3 Anisotropy of Magnetic Susceptibility Results

The results of AMS analysis are summarized in Table 1. Of the 177 block samples, 6 were rejected due to anomalously broad principal susceptibility axes that were associated localised hydrothermal alteration. The principal parameters used to characterize magnetic anisotropy are the Corrected Anisotropy Degree ($P_j = \{2[(\eta_1 - \eta)^2 + (\eta_2 - \eta)^2 + (\eta_3 - \eta)^2]\}$ after Jelinek (1981)) and Shape Factor ($T_j = [2\eta_2 - \eta_1 - \eta_3] / [\eta_1 - \eta_3]$ after Jelinek (1981)), Total Anisotropy ($H = [K1-K3] / K_{mean}$) after Owens (1974)) and mean susceptibility ($K_m = [K1+K2+K3] / 3$) (see Tarling & Hrouda (1993)).

Mean susceptibility (K_{mean}) values across the pluton range from 1.206×10^{-3} - 24.083×10^{-3} (SI units), these values average at $14.448 \times 10^{-3} \pm 4.387 \times 10^{-3}$. A contour map of K_{mean} across the intrusion illustrates a lack of anomalous magnetic susceptibility across G1-G2 facies contacts or the inner strain

zone (Fig. 5); this indicates a reasonably homogeneous distribution and composition of magnetite within the pluton. The average degree of anisotropy (H) (Owens 1974) is 13% ± 6.8% and varies between 3.96% and 33.8%.

Figure 5

A contour map of the Corrected Degree of Anisotropy (P_j) shows a systematic distribution of magnetic anisotropy (Fig. 6a) where low P_j values are recorded in the core and much higher P_j values (max 1.25) are recorded around the periphery of the pluton. Along the margin of the intrusion elevated P_j values (min. 1.02) are concentrated in the ENE and WSW that contrast low P_j values near NNW and SSE contacts. Of 171 AMS ellipsoids measured, 21 are dominantly prolate and 150 are dominantly oblate and Shape Factor (T_j) values vary between -0.71 and 0.97. A contour map of T_j across the pluton shows a very systematic distribution of T_j values (Fig. 6b). A suite of prolate to triaxial tensors ($0.3 \geq T_j \geq -0.7$) extend along a NNW-SSE axis and define a zone distinct from those areas to the east and west. The marginal areas of the pluton are dominated by oblate magnetic fabrics, these are most pronounced in the east and west and, again, are weakest along the intrusions NNW-SSE axis (Fig. 6b).

Figure 6

Finally, in accordance with field observations two zones with anomalously oblate T_j values are recorded in the east and west 2km from the country rock contact (Fig. 6b). These define NNW-SSE oriented arcs with T_j values between 0.54-0.97 (Average T_j = 0.7) which is significantly higher than the average T_j value recorded for tensors about the periphery (Average T_j = 0.45).

4.4 Attitude and Distribution of Magnetic Fabrics

The attitude, distribution and shape of AMS fabrics with representative stereographic projections of averaged principal AMS axes are presented in (Fig. 7). Stereographic projections of AMS data reveal that, for the majority of samples, determined K1, K2 and K3 axes are extremely well constrained (Fig. 7). After Jelinek (1981), Owens (2000a) and Owens (2000b), AMS ellipsoids that are interpreted as dominantly prolate and oblate are depicted as lineations and foliations respectively and L-S fabrics are plotted using both lineation and foliation symbols (Fig. 7).

Figure 7

Prolate fabrics are concentrated in the core of the intrusion, plunge moderate - steeply and strike NNW-SSE, parallel to G2 sheets in the pluton and D5 faults in the country rock (labelled Z in Fig. 7). Oblate tensors detected in the centre of the plutons have characteristically low T_j and P_j values. Despite the circular shape of the pluton, oblate fabrics between the core of the intrusion and periphery define a NNW-SSE ellipsoid symmetry. Corresponding stereographic projections characteristically exhibit tight K3 axes and girdles defined by K1 and K2 axes (labelled Y in Fig. 7). At map scale, these steep foliations collectively define a crude ellipsoid symmetry elongate along a NNW-SSE axis. This geometry is anomalous when compared to adjacent marginal foliations that have tightly constrained K1, K2 and K3 axes and define a steeply outward inclined concentric foliation (labelled X in Fig. 7). Respective K1 vectors plunge moderately to steeply outwards and are consistent with sub-vertical stretching.

5 Discussion

Rock magnetic data are discussed below in light of pertinent petrographic, field and regional geological data.

5.1 Characterisation of Magnetic Mineralogy and Significance of AMS

The magnetic anisotropy of a rock depends on the anisotropies of individual grains in the sample and the degree of alignment of these grain anisotropies (Tarling & Hrouda 1993). Minerals with higher magnetic susceptibility and anisotropy values are more likely to dominate the AMS tensor and it is therefore important to evaluate the contribution made to the net tensor by each phase and also the geometrical relationship between of these phases. Petrographic data show the modal abundance of paramagnetic phases in both facies is below 10% and average K_{mean} values (Table 1) are of the order $14.448 \times 10^{-3} \pm 4.133 \times 10^{-3}$. These data indicate that a high susceptibility ferromagnetic phase dominates the AMS tensor and the contribution from paramagnetic minerals will, in general, be negligible (Tarling & Hrouda 1993, Hrouda & Kahan 1991). These data are supported by cryogenic data (Fig. 4b) that show a minimal paramagnetic contribution to bulk susceptibility and a strong ferromagnetic signature under low and room temperature conditions. High temperature susceptibility experiments consistently return T_C values between 575-580°C which infer a low Ti titanomagnetite (near stoichiometric magnetite) is the principal ferromagnetic phase in this case (Lattard *et al.* 2006, Akimoto 1962).

Inverse or intermediate magnetic fabrics can occur where fine grained single domain (SD) magnetite is present in a rock sample (Potter & Stephenson 1988); it is therefore important to constrain the principal

ferromagnetic grain size and inferred domain state in the case of magnetite. The shape of high temperature vs. susceptibility curves may be used as a proxy for magnetic grain size (Orlický 1990, Liss *et al.* 2004). Here, a lack of a distinct SD like Hopkinson Peaks in all specimens indicate that multidomain magnetite is most likely the dominant ferromagnetic phase in both facies. SIRM acquisition curves show 95% saturation is reached in <0.3T and BIRM results show reasonably low H_{CR} values of <0.062T (Fig. 4c). Lowrie-Fuller test experiments return exponential demagnetisation curves and MDF values of <20mT (Fig. 4d). Together these data indicate a magnetically soft ferromagnetic phase, such as PSD to MD titanomagnetite, is the primary carrier of magnetic remanence in the studied samples (Dunlop 1986, Xu & Dunlop 1995, Lowrie & Fuller 1971, Argyle & Dunlop 1990, Bailey & Dunlop 1983).

Petrographic observations identify surficial oxidisation (maghemitization) within coarse grained magnetite (Fig. 3c) and no significant volume of sulphides in the studied samples. Maghemitization is a low temperature topotactic transformation process involving the oxidization of titanomagnetite to titanomaghemite or magnetite to maghemite (Kachi *et al.* 1963). Maghemitization occurs via the diffusion of Fe^{2+} from the crystal interior to the crystal surface where it is converted to Fe^{3+}, thus increasing the Ti:Fe ratio (Dunlop & Özden 1997). This process causes fracturing and associated surficial oxidization of coarse parent iron oxide phase (Cui *et al.* 1994, Colombo *et al.* 1964), as is observed in Figure 3c. High temperature susceptibility curves show a distinct "bump" in susceptibility (~5-10%) at ~300°C that is not present on the cooling curve and a net increase in susceptibility (~10-20%) is typical on cooling to room temperature (Fig. 4a). RD25 exhibits a 100% increase in susceptibility after cooling and lacks a 300°C bump along the heating curve, indicating that this sample does not contain sulphides but probably contains titanomaghemite. Titanomaghemite is unstable and will invert to magnetite and ilmenite at ~ 300°C in oxidizing conditions (Hrouda 2003, Hrouda *et al.* 2006, Magee *et al.* 2012, Petronis *et al.* 2011, Dunlop & Özden 1997). Accordingly, we interpret the above as the breakdown of titanomaghemite at ~300°C and the growth of a new ferromagnetic phase (magnetite) at high temperature. Such a phase change causes a net increase in bulk susceptibility owing to the formation of magnetite from less susceptible titanomaghemite which causes a shift in the cooling curve relative to that of the heating curve (Petronis *et al.* 2011).

Tight AMS principal axes confidence ellipses and reproducibility of results between duplicate sites demonstrates the reliability of the presented AMS data set. A high degree of consistency is observed between contact parallel foliations reported by Leake (1969) and detected AMS foliations in the same area. Petrographic observations show the orientation of titanomagnetite is controlled by the orientation of silicate minerals and that detected AMS fabrics replicate the observed silicate and iron oxide petrographic

fabric (Fig. 3c). Rock magnetic data, particularly cryogenic magnetic susceptibility data, show paramagnetic phases are essentially fully masked by high susceptibility titanomagnetite at room temperature (Fig. 4b). Principal susceptibility axis are typically well constrained in both normalized and un-normalized projections (Owens 2000b) and there is no microstructural evidence of post sub-magmatic state fabric overprints. We therefore conclude that AMS tensors are "normal" (Rochette *et al.* 1999, Ferré 2002) and that these tensors are representative of true petrographic fabrics that pertain to strain imparted during pluton construction (Hrouda *et al.* 1971, Heller 1973). These findings are consistent with those of several other studies on granitoids of similar grain size (e.g. Ferre *et al.* (1999), Petronis *et al.* (2004) and Martins *et al.* (2011))

5.2 Internal Architecture of the Pluton

Concentric steeply inclined oblate foliations and lineations within 200m of the pluton contact are interpreted as sub-magmatic fabrics associated with the laccolith inflation process (Fig. 8). Distinct from this, a broad inner shear zone is recognized ~2km from the pluton's margin that defines an overall NNW-SSE elongate ellipsoid in map view (Fig. 8a). A contoured stereographic projection of K3 AMS principal susceptibility axes compiled from the inner strain zone shows that a very high proportion of foliations in this area are steeply inclined and strike NNW-SSE (Fig. 8b). A preferential distribution of K1 axes along the NNW-SSE axes of the composite stereonet also demonstrates the internal NNW-SSE anisotropy in this circular intrusion (Fig. 8b). A polar plot comparing anisotropy in the inner shear zone to that of the peripheral fabric shows shape anisotropy is much higher than elsewhere in the intrusion and strongly oblate within the inner shear zone (Fig. 8c). Stereographic projections of individual AMS sample sites in this zone show a girdle distribution of K1 and K2 axes that define a magnetic foliation (Fig. 8) and a contour map that shows relatively elevated T_j values (Fig. 6b) within the inner strain zone. Petrographic analysis indicate that the observed fabrics formed in the high temperature sub-magmatic state and no changes in rock mode, grain size or magnetic bulk susceptibility are noted across this area. Therefore, this fabric anomaly is interpreted to reflect the preferential distribution of strain along a NNW-SSE axis during the emplacement process rather than a subtle intrusive contact or the preferential distribution of ferromagnetic minerals.

Figure 8

The interior of the pluton appears texturally isotropic in the field however AMS analysis yields an overall low to moderate degree of magnetic anisotropy in this area (H = 4-12%). A polar plot of P_j vs. T_j shows

that a high proportion of AMS tensors from the plutons interior are prolate (Fig. 8c) and a stereographic projection of K1 axes shows that these magnetic lineations are steeply inclined and preferentially trend NNW-SSE (Fig. 8a, b). The parallel geometric relationship between the detected magnetic anisotropy, NNW-SSE faults in the country rock (Harvey 1967) and the orientation of G2 sheets within the pluton is emphasised. Furthermore, petrographic analysis demonstrates that the observed anisotropy was imparted in the magmatic state and lobate contacts indicate the near contemporaneous emplacement of G1 and G2. Accordingly, we suggest that the detected magnetic fabrics reflect magma ascent to the site of emplacement via some pre-existing D5 NNW-SSE conduit that underlies the centre of the Roundstone Pluton.

6 An Emplacement Model for the Roundstone Pluton

Stoping describes a process where a volume of magma, equal to the volume of a detached country rock block, is displaced upwards as detached blocks descend (density permitting). Paterson and Fowler (1993) consider stoping to be an important Material Transfer Process (MTP) in agreement with other authors who consider it a valid emplacement mechanism (e.g. Compton (1955), Snowden and Snowden (1981), Marsh (1982), Galadí-Enríquez *et al.* (2003), Burchardt *et al.* (2009) and Burchardt *et al.* (2012)). Recently, Leake (2011) also cited stoping as a major process during the emplacement of the Roundstone pluton.

Fundamental problems are associated with stoping as an emplacement process (see Hutton (1996) and Glazner and Bartley (2006) but also Glazner and Bartley (2008), Yoshinobu and Barns (2008), Clarke and Erdmann (2008)). Among these are heat transfer issues associated with an increase in country rock - magma surface area exposure (Hutton 1996), lack of evidence for large masses of stoped blocks at the base of magma chambers (Marsh 1982, Buddington 1959), and a lack of large scale assimilation of country rock into granitic melts where stoping is said to have occurred (Pitcher 1987, Ague & Brimhall 1988, Miller *et al.* 1988). Most notable is the space problem i.e. detachment of ordered blocks and random deposition of these at the base of a magma chamber will ultimately stall upward migration of a pluton as magma is left to infill interstitial space between detached blocks.

In the current example, stoping as a mechanism does not explain the occurrence of a steep circular faulted contact, a NNW-SSE orientated sub-magmatic elliptical zone of oblate fabrics, the nature of NNW-SSE vertical G2 sheets or the near perfect circular foot print of the intrusion (stoping should exploit pre-existing ESE-WNW grain of the country rock). The interior of the pluton also lacks country rock xenoliths. Buoyancy driven ascent is unlikely as the footwall of the Mannin Thrust, through which

granodioritic magma must have ascended, is rhyolitic (Leake & Singh 1986, Draut & Clift 2002) and therefore less dense than the ascending granodiorite magma. For these reasons, stoping as a mechanism of emplacement is refuted in this situation and more generally as a feasible emplacement process; it is a localized result of, rather than a mechanism for, magma ingress.

Corry (1988) describes a punched laccolith as a pluton with a flat base and roof, bound by steep or vertical peripheral faults that assumes a crude cylindrical shape. Characteristic traits include a brittle bounding margin, minimal distortion to the host rock close to the faulted contact, occasional small scale laterally discontinuous dykes parallel to the contact, a close to circular outline and an epizonal level of emplacement (Gilbert 1877, Hunt 1958, Koch *et al.* 1981, Cruden 2008). The above describe features of the Roundstone Pluton meet these criteria and a comparison of data from the Omey Pluton and the Carna Pluton indicate that the Roundstone Pluton was likely emplaced into the epizone between 4-8km (Ferguson & Harvey 1979, Gallagher *et al.* 1992, Ahmed-Said & Leake 1996). Goulty and Schofield (2008) argue that sub-circular saucer shaped intrusions, that are symmetrically similar to Roundstone Pluton, are fed by steeply inclined dykes that lie directly below the observed intrusion and strike parallel to their long axis. We propose that a punched laccolith model is consistent with the field, petrographic and geophysical data discussed above.

6.1 Interaction between Regional Transpression and Local Structures

Physical barriers, such as a defined parting surface, coupled with the reduced effects of lithostatic load at shallow depth, are capable of "capping" ascent conduits and forcing lateral emplacement of magma (Mudge 1968). The intersection of a horizontal structural dislocation with a propagating vertical ascent conduit may also serve to re-orientate the local stress field and promote a transition from ascent to emplacement (Weertman 1980, Engelder & Sbar 1984).

The Connemara Metamorphic Complex is the hanging wall to a regional thrust in which the Mannin Thrust is the fault plane and the Delaney Dome Fm. is the foot wall (Fig. 2). Leake and Tanner (1994) show that NNW-SSE D5 faults propagate through the foot wall into the Connemara Metamorphic Complex and that these faults pre-date late Caledonian magmatism in Connemara. New data presented here that show these structures off-set the contacts of the Roundstone Pluton and control much of the internal architecture of the pluton. This indicates that these structures were reactivated during late Caledonian strike slip and contemporaneous magmatism (Feely *et al.* 2010, McCarthy 2013). We propose that reactivated NNW-SSE faults acted as magma ascent conduits during ~420Ma regional transpression

and that these conduits intersected and abutted against the Mannin Thrust at the level of emplacement. Significant competency contrasts between hanging wall and footwall materials, along with the inherent weakness of this lateral planar discontinuity, acted as a stress barrier to form an approximately axi-symmetric stress field in the host rock in which $\sigma 3$ was vertical and $\sigma 1 \sim 2\sigma > 3\sigma$. This scenario promoted the lateral emplacement of a broadly disk shaped intrusion directly over the NNW-SSE sub-vertical planar ascent structure.

6.2 Mechanism of Emplacement

A sub-vertical NNW-SSE D5 fault provided a plane of weakness which abutted against the sub-horizontal Mannin Thrust (Fig. 9a). Excess magma pressure and the ambient stress field promoted dilation across this subvertical fault that facilitated the ascent of batches of magma; reduced hydrostatic pressure at shallower levels in the crust allowed the Mannin Thrust to act as a stress barrier and instigate lateral emplacement of magma (Fig. 9b). Lateral emplacement of magma initially occurred as a thin sheet that extended to the full diameter of the intrusion to form a disk shape prior to vertical inflation (Pollard & Johnson 1973, Corry 1988, Petronis *et al.* 2004). Early emplacement was driven by excess magma pressure and was facilitated by ductile up-doming of the bounding roof that accommodated pluton inflation (Fig. 9c). Internal lateral emplacement fabrics became overprinted by progressively inclined oblate strain tensors as magma became packed into the site of emplacement (Fig. 9c). Progressive inflation increased radial tensile strain in the roof resulting in brittle failure around the periphery to form a cylindrical fault bound intrusion under a block of vertically displaced country rock (Fig. 9d). Inflation continued until hydrostatic pressure from the overlying block equalled the force exerted by upwelling magma (Corry 1988). Stoped contacts observed in the field represent localities where magma intruded into the peripheral bounding faults and incorporated local blocks of country rock. The final phase of pluton construction involved the ascent of a plexus of G2 sheets, again via NNW-SSE conduits, and the lateral emplacement of this magma into the semi-molten G1 magma (Fig. 9d). Post-failure relaxation of the country rock generated a subtle pluton-up shear sense expressed as a contact-parallel stretching direction that is recorded by steeply outward dipping K1 axes near the pluton - country rock contact.

These processes resulted in the development of a cylindrical laccolith which is morphologically similar to a bysmalith with gently outward dipping external contacts (Habert & De Saint-Blanquat 2004, Horsman *et al.* 2010). However, having an up-faulted roof, this intrusion is best described as a punched laccolith (Corry 1988).

Figure 9

7 Conclusions

The Roundstone Pluton is a punched laccolith. Deep-seated NNW-SSE D5 faults are prominent features of the footwall of the Mannin Thrust that became reactivated during regional sinistral transpression between the late Silurian and early Devonian, magma ascent occurred along these faults. The Mannin Thrust acted as a flat-lying effective epizone stress barrier that instigated lateral emplacement. Pluton inflation culminated in the radial failure of the roof rock and formation of a sub-circular laccolith elongate parallel to the NNW-SSE feeder conduit.

These data demonstrate that separate ascent and emplacement processes can be identified and that diapirism is therefore untenable for this intrusion. Such an approach could usefully be undertaken on other plutons where existing field data are incapable of unequivocally resolving controversy regarding pluton construction processes.

9 Acknowledgements

Conrad Daly and John McCarthy are acknowledged for donating their time and technical expertise during field and analytical work. We would like to thank the local community at Roundstone, Co. Galway, particularly Ruth Hunt and Jon Hunt for their continued hospitality throughout this study. Martin Feely, Bernard Leake, Dave McCarthy and Pat Meere are thanked for their insightful critique during the project. The authors would like to thank the reviewers of helpful comments. McCarthy acknowledges receipt of an Irish Research Council for Science Engineering and Technology (IRCSET) Grant and a National University of Ireland Travelling Studentship for postgraduate study at University College Cork.

References Cited

AGUE, J.J. & BRIMHALL, G.H. 1988. Magmatic arc asymmetry and distribution of anomalous plutonic belts in the batholiths of California: Effects of assimilation, crustal thickness, and depth of crystallization. *Geological Society of America Bulletin*, **100**, 912–927, doi: 10.1130/0016-7606(1988)100<0912:maaado>2.3.co;2.

AHMED-SAID, Y. & LEAKE, B.E. 1996. The conditions of metamorphism of a grossular - wollastonite vesuvianite skarn from the Omey Granite, Connemara, western Ireland, with special reference to the chemistry of vesuvianite. *Mineralogical Magazine*, **60**, 541–550.

AKIMOTO, S. 1962. Magnetic properties of FeO-Fe2O3-TiO2 system as a basis of rock magnetism. *Journal of Physics Society Japan*, **17 Suppl.**, 706–710.

ALMQVIST, B.S., HERWEGH, M., SCHMIDT, V., PETTKE, T. & HIRT, A.M. 2010. Magnetic susceptibility as a tool to study deformed calcite with variable impurity content. *Geochem. Geophys. Geosyst.*, **11**, Q01Z09, doi: 10.1029/2009gc002900.

ANDERSON, E.M. 1936. The dynamics of the formation of cone sheets, ring dikes and cauldron subsidence. *Royal Society of Edinburgh Proceedings*, **56**, 128–157.

ARGYLE, K.S. & DUNLOP, D.J. 1990. Low-Temperature and High-Temperature Hysteresis of Small Multidomain Magnetites (215-540 nm). *Journal of Geophysical Research*, **95**, 7069–7082, doi: 10.1029/JB095iB05p07069.

AUBOURG, C. & ROBION, P. 2002. Composite ferromagnetic fabrics (magnetite, greigite) measured by AMS and partial AARM in weakly strained sandstones from western Makran, Iran. *Geophysical Journal International*, **151**, 729–737, doi: 10.1046/j.1365-246X.2002.01800.x.

BAILEY, M.E. & DUNLOP, D.J. 1983. Alternating field characteristics of pseudo-single-domain (2–14 μm) and multidomain magnetite. *Earth and Planetary Science Letters*, **63**, 335–352, doi: 10.1016/0012-821x(83)90108-5.

BATEMAN, R. 1985. Aureole deformation by flattening around a diapir during in-situ ballooning: the Cannibal Creek granite. *Journal of Geology*, **93**, 293–310.

BENJAMIN, R.E.K. 1968. The quartz plagioclase gneisses of Western Connemara, Ireland. *Geological Magazine*, **105**, 456–470.

BORRADAILE, G.J. & JACKSON, M. 2010. Structural geology, petrofabrics and magnetic fabrics (AMS, AARM, AIRM). *Journal of Structural Geology*, **32**, 1519–1551, doi: 10.1016/j.jsg.2009.09.006.

BOUCHEZ, J.L. 1997. Granite is never isotropic: an introduction to AMS studies of granitic rocks. *In: Bouchez, J.L., Hutton, D.H.W., Stephens, W.E., (eds.), Grantie: From Segregation of Melt to Emplacement Fabrics, Kluwer Academic Publishers, Dordrecht*, 95–112.

BOUCHEZ, J.L., DELAS, C., GLEIZES, G., NÉDÉLEC, A. & CUNEY, M. 1992. Submagmatic microfractures in granites. *Geology*, **20**, 35–38, doi: 10.1130/0091-7613(1992)020<0035:smig>2.3.co;2.

BOUCHEZ, J.L., NGUEMA, T.M.M., ESTEBAN, L., SIQUEIRA, R. & SCRIVENER, R. 2006. The tourmaline-bearing granite pluton of Bodmin (Cornwall, UK): magnetic fabric study and regional inference. *Journal of the Geological Society*, **163**, 607–616, doi: 10.1144/0016-764905-104.

BRUN, J.P., GAPAIS, D., COGNE, J.P., LEDRU, P. & VIGNERESSE, J.L. 1990. The Flamanville Granite (Northwest France): An unequivocal example of a syntectonically expanding pluton. *Geological Journal*, **25**, 271–286, doi: 10.1002/gj.3350250310.

BUDDINGTON, A.F. 1959. Granite emplacement with special reference to North America. *Bulletin of the Geological Society of America*, **70**, 671–747.

BURCHARDT, S., TANNER, D.C., KRUMBHOLZ, M. & GEOSCIENCE, A. 2009. Emplacement of the Slaufrudalur Pluton, southeast Iceland, deduced from field observations and its three-dimensional shape. *Trabajos de Geología, Universidad de Oviedo*, **29**, 129–130.

BURCHARDT, S., TANNER, D. & KRUMBHOLZ, M. 2012. The Slaufrudalur pluton, southeast Iceland—An example of shallow magma emplacement by coupled cauldron subsidence and magmatic stoping. *Geological Society of America Bulletin*, **124**, 213–227, doi: 10.1130/b30430.1.

BUROV, E., JAUPART, C. & GUILLOU-FROTTIER, L. 2003. Ascent and emplacement of buoyant magma bodies in brittle-ductile upper crust. *Journal of Geophysical Research*, **108**, 2177, doi: 10.1029/2002jb001904.

CANON-TAPIA, E. 1996. Single-grain versus distribution anisotropy: a simple three-dimensional model. *Physics of the Earth and Planetary Interiors*, **94**, 149–158.

CAÑÓN-TAPIA, E. 2001. Factors affecting the relative importance of shape and distribution anisotropy in rocks: theory and experiments. *Tectonophysics*, **340**, 117–131, doi: 10.1016/S0040-1951(01)00150-0.

CHADIMA, M., CAJZ, V. & TÝCOVÁ, P. 2009. On the interpretation of normal and inverse magnetic fabric in dikes: Examples from the Eger Graben, NW Bohemian Massif. *Tectonophysics*, **466**, 47–63, doi: 10.1016/j.tecto.2008.09.005.

CLARK, D.A. 1984. Hysteresis properties of sized dispersed monoclinic pyrrhotite grains. *Geophysical Research Letters*, **11**, 173–176, doi: 10.1029/GL011i003p00173.

CLARKE, D.B. & ERDMANN, S. 2008. Is stoping a volumetrically significant pluton emplacement process?: Comment. *Geological Society of America Bulletin* , **120** , 1072–1074, doi: 10.1130/B26147.1.

CLOUGH, C.T., MAUFE, H.B. & BAILEY, E.B. 1909. The Cauldron-Subsidence of Glen Coe, and the Associated Igneous Phenomena. *Quarterly Journal of the Geological Society*, **65**, 611–653,NP,655–657,NP,659–669,NP,671–678, doi: 10.1144/gsl.jgs.1909.065.01-04.35.

COLEMAN, D.S., GRAY, W. & GLAZNER, A.F. 2004. Rethinking the emplacement and evolution of zoned plutons: Geochronologic evidence for incremental assembly of the Tuolumne Intrusive Suite, California. *Geology*, **32**, 433, doi: 10.1130/G20220.1.

COLOMBO, U., FAGHERAZZI, G., GAZZARRINI, F., LANZAVECCHI, G. & SIRONI, G. 1964. Mechanisms in the First Stage of Oxidation of Magnetites. *Nature*, **202**, 175–176.

COMPTON, R. 1955. Trondhjemite batholith near Bidwell Bar, California. *Bulletin of the Geological Society of America*, **66**, 9–44.

CORRY, C.E. 1988. Laccoliths: Mechanics of emplacement and growth. *Geological Society of America*, 3–10.

COURRIOUX, G. 1987. Oblique diapirism: the criffel granodiorite/granite zoned pluton (southwest Scotland). *Journal of Structural Geology*, **9**, 313–330, doi: 10.1016/0191-8141(87)90055-1.

CRUDEN, A.R. 2008. Report for Svensk Kärnbränslehantering AB. *Swedish Nuclear Fuel and waste Management Co.*

CUI, Y., VEROSUB, K.L. & ROBERTS, A.P. 1994. The effect of low-temperature oxidation on large multi-domain magnetite. *Geophysical Research Letters*, **21**, 757–760, doi: 10.1029/94GL00639.

DALY, R.A. 1933. Igneous rocks in the depths of the earth. *McGraw Hill, New York*.

DEKKERS, M.J. 1988. Magnetic properties of natural pyrrhotite Part I: Behaviour of initial susceptibility and saturation-magnetization-related rock-magnetic parameters in a grain-size dependent framework. *Physics of the Earth and Planetary Interiors*, **52**, 376–393, doi: http://dx.doi.org/10.1016/0031-9201(88)90129-X.

DRAUT, A.E. & CLIFT, P.D. 2002. The origin and significance of the Delaney Dome Formation, Connemara, Ireland. *Journal of the Geological Society*, **159**, 95–103, doi: 10.1144/0016-764901034.

DUNLOP, D.J. 1972. Magnetic Mineralogy of Unheated and Heated Red Sediments by Coercivity Spectrum Analysis*. *Geophysical Journal of the Royal Astronomical Society*, **27**, 37–55, doi: 10.1111/j.1365-246X.1972.tb02346.x.

DUNLOP, D.J. 1986. Hysteresis Properties of Magnetite and their Dependence on Particle Size: A Test of Pseudo-Single-Domain Remanence Models. *Journal of Geophysical Research*, **91**, 9569–9584, doi: 10.1029/JB091iB09p09569.

DUNLOP, D.J. & ÖZDEN, Ö. 1997. *Rock Magnetism*. Cambridge University Press.

DUNLOP, D.J., HANES, J.A. & BUCHAN, K.L. 1973. Indices of Multidomain Magnetic Behavior in Basic Igneous Rocks: Alternating-Field Demagnetization, Hysteresis, and Oxide Petrology. *Journal of Geophysical Research*, **78**, 1387–1393.

ENGELDER, T. & SBAR, M.L. 1984. Near-surface in situ stress: Introduction. *Journal of Geophysical Research: Solid Earth*, **89**, 9321–9322, doi: 10.1029/JB089iB11p09321.

ENGLAND, R.W. 1990. The identification of granitic diapirs. *Journal of the Geological Society*, **147**, 931–933, doi: 10.1144/gsjgs.147.6.0931.

EVANS, B.W. & LEAKE, B.E. 1970. The Geology of the Toombeola District, Connemara, Co. Galway. *Proceedings of the Royal Irish Academy. Section B: Biological, Geological, and Chemical Science*, **70**, 105–140.

FANJAT, G., CAMPS, P., SHCHERBAKOV, V., BAROU, F., SOUGRATI, M.T. & PERRIN, M. 2012. Magnetic interactions at the origin of abnormal magnetic fabrics in lava flows: a case study from Kerguelen flood basalts. *Geophysical Journal International*, **189**, 815–832, doi: 10.1111/j.1365-246X.2012.05421.x.

FEELY, M., SELBY, D., HUNT, J. & CONLIFFE, J. 2010. Long-lived granite-related molybdenite mineralization at Connemara, western Irish Caledonides. *Geological Magazine*, **147**, 886–894, doi: 10.1017/s0016756810000324.

FERGUSON, C.C. & HARVEY, P.K. 1979. Thermally overprinted Dalradian rocks near Cleggan, Connemara Western Ireland. *Proceedings of the Geologists' Association*, **90**, 43–50, doi: 10.1016/s0016-7878(79)80030-9.

FERRÉ, E.C. 2002. Theoretical models of intermediate and inverse AMS fabrics. *Geophysical Research Letters*, **29**, 1127, doi: 10.1029/2001gl014367.

FERRÉ, E.C., WILSON, J. & GLEIZES, G. 1999. Magnetic susceptibility and AMS of the Bushveld alkaline granites, South Africa. *Tectonophysics*, **307**, 113–133, doi: http://dx.doi.org/10.1016/S0040-1951(99)00122-5.

FORIEN CARLO, M. 2009. Simultaneously ascending diapirs from different depths and different positions: a centrifuge study. *Geotectonic Research*, **96**, 39–52.

FRIEDRICH, A.M., HODGES, K. V, BOWING, S.A. & MARTIN, M.W. 1999a. Geochronological constraints on the magmatic, metamorphic and thermal evolution of the Connemara Caledonides, western Ireland. *Journal of the Geological Society*, **156**, 1217–1230, doi: 10.1144/gsjgs.156.6.1217.

FRIEDRICH, A.M., BOWRING, S.A., MARTIN, M.W. & HODGES, K. V. 1999b. Short-lived continental magmatic arc at Connemara, western Irish Caledonides: Implications for the age of the Grampian orogeny. *Geology*, **27**, 27–30, doi: 10.1130/0091-7613(1999)027<0027:slcmaa>2.3.co;2.

GAILLOT, P., DE SAINT-BLANQUAT, M. & BOUCHEZ, J.-L. 2006. Effects of magnetic interactions in anisotropy of magnetic susceptibility: Models, experiments and implications for igneous rock fabrics quantification. *Tectonophysics*, **418**, 3–19, doi: 10.1016/j.tecto.2005.12.010.

GALADÍ-ENRÍQUEZ, E., GALINDO-ZALDÍVAR, J., SIMANCAS, F. & EXPÓSITO, I. 2003. Diapiric emplacement in the upper crust of a granitic body: the La Bazana granite (SW Spain). *Tectonophysics*, **361**, 83–96, doi: 10.1016/s0040-1951(02)00562-0.

GALLAGHER, V., FEELY, M., HÖGELSBERGER, H., JENKIN, G.R.T. & FALLICK, A.E. 1992. Geological, fluid inclusion and stable isotope studies of Mo mineralization, Galway Granite, Ireland. *Mineralium Deposita*, **27**, 314–325, doi: 10.1007/BF00193402.

GILBERT, G.K. 1877. Report on the geology of the Henry Mountains (Utah). *United States Geological Survey, Washington D.C.*

GLAZNER, A.F. & BARTLEY, J.M. 2006. Is stoping a volumetrically significant pluton emplacement process? *Geological Society of America Bulletin*, **118**, 1185–1195, doi: 10.1130/B26312.1.

GLAZNER, A.F. & BARTLEY, J.M. 2008. Reply to comments on 'Is stoping a volumetrically significant pluton emplacement process?' *Geological Society of America Bulletin* , **120** , 1082–1087, doi: 10.1130/B26312.1.

GOULTY, N.R. & SCHOFIELD, N. 2008. Implications of simple flexure theory for the formation of saucer-shaped sills. *Journal of Structural Geology*, **30**, 812–817, doi: http://dx.doi.org/10.1016/j.jsg.2008.04.002.

HABERT, G. & DE SAINT-BLANQUAT, M. 2004. Rate of construction of the Black Mesa bysmalith, Henry Mountains, Utah. *Geological Society, London, Special Publications* , **234** , 163–173, doi: 10.1144/GSL.SP.2004.234.01.10.

HARGRAVES, R.B., JOHNSON, D. & CHAN, C.Y. 1991. Distribution anisotropy: The cause of AMS in igneous rocks? *Geophysical Research Letters*, **18**, 2193–2196, doi: 10.1029/91gl01777.

HARKER, A. 1909. The Natural History of Igenous Rocks. *Cambridge University Press*.

HARVEY, K.P. 1967. The Geology of the Glinsk District, Connemara, Eire. *PhD Thesis, University of Bristol, UK*.

HE, B., XU, Y.-G. & PATERSON, S. 2009. Magmatic diapirism of the Fangshan pluton, southwest of Beijing, China. *Journal of Structural Geology*, **31**, 615–626, doi: 10.1016/j.jsg.2009.04.007.

HEIDER, F., DUNLOP, D.J. & SOFFEL, H.C. 1992. Low-Temperature and Alternating Field Demagnetization of Saturation Remanence and Thermoremanence in Magnetite Grains (0.037 μm to 5 mm). *Journal of Geophysical Research*, **97**, 9371–9381, doi: 10.1029/91jb03097.

HELLER, F. 1973. Magnetic anisotropy of granitic rocks of the Bergell massif (Switzerland). *Earth and Planetary Science Letters*, **20**, 180–188, doi: http://dx.doi.org/10.1016/0012-821X(73)90156-8.

HIRTH, G. & TULLIS, J. 1992. Dislocation creep regimes in quartz aggregates. *Journal of Structural Geology*, **14**, 145–159, doi: 10.1016/0191-8141(92)90053-Y.

HOLDER, M.T. 1979. An emplacement mechanism for post tectonic granites and its implications for their geochemical features. *In: Atherton, M.P., Tarney, J., (eds)., Origin of granite batholiths: geochemical evidence. Shiva Publishing*, 116–128.

HOPKINSON, J. 1890. Magnetic Properties of Alloys of Nnickel and Iron. *Proceedings of the Royal Society of London*, **48**, 1–13.

HORSMAN, E., MORGAN, S., DE SAINT-BLANQUAT, M., HABERT, G., NUGENT, A., HUNTER, R.A. & TIKOFF, B. 2010. Emplacement and assembly of shallow intrusions from multiple magma pulses, Henry Mountains, Utah. *Geological Society of America Special Papers*, **472**, 117–132, doi: 10.1130/2010.2472(08).

HROUDA, F. 2003. Indices for Numerical Characterization of the Alteration Processes of Magnetic Minerals Taking Place During Investigation of Temperature Variation of Magnetic Susceptibility. *Studia Geophysica et Geodaetica*, **47**, 847–861, doi: 10.1023/a:1026398920172.

HROUDA, F. & KAHAN, S. 1991. The magnetic fabric relationship between sedimentary and basement nappes in the High Tatra Mountains, N. Slovakia. *Physics of the Earth and Planetary Interiors*, **63**, 71–77.

HROUDA, F., CHLUPÁČOVÁ, M. & REJL, L. 1971. The mimetic fabric of magnetite in some foliated granodiorites, as indicated by magnetic anisotropy. *Earth and Planetary Science Letters*, **11**, 381–384, doi: 10.1016/0012-821x(71)90198-1.

HROUDA, F., CHLUPÁČOVÁ, M. & MRÁZOVÁ, Š. 2006. Low-field variation of magnetic susceptibility as a tool for magnetic mineralogy of rocks. *Physics of the Earth and Planetary Interiors*, **154**, 323–336, doi: 10.1016/j.pepi.2005.09.013.

HUNT, C.B. 1958. Structural and igneous geology of the La Sal Mountains, Utah. *United States Geological Survey, Progessional Paper*, **294**, 305–364.

HUTTON, D.H.W. 1988. Granite emplacement mechanisms and tectonic controls: inferences from deformation studies. *Earth and Environmental Science Transactions of the Royal Society of Edinburgh*, **79**, 245–255, doi: doi:10.1017/S0263593300014255.

HUTTON, D.H.W. 1990. A new mechanism of granite emplacement: intrusion in active extensional shear zones. *Nature*, **343**, 452–455.

HUTTON, D.H.W. 1996. The 'space problem' in the emplacement of granite. *Episodes, International Union of Geological Sciences*, **19**, 114–119.

HUTTON, D.H.W. & REAVY, R.J. 1992. Strike-slip tectonics and granite petrogenesis. *Tectonics*, **11**, 960–967, doi: 10.1029/92tc00336.

HUTTON, D.H.W. & SIEGESMUND, S. 2001. The Ardara Granite: Reinflating the Balloon Hypothesis. *Zeitschrift der Deutschen Geologischen Gesellschaft*, **152**, 309–323.

JACQUES, J.M. & REAVY, R.J. 1994. Caledonian plutonism and major lineaments in the SW Scottish Highlands. *Journal of the Geological Society*, **151**, 955–060.

JELINEK, V. 1981. Characterization of the magnetic fabric of rocks. *Tectonophysics*, **79**, T63–T67, doi: 10.1016/0040-1951(81)90110-4.

JOHNSON, S.E.E., FLETCHER, J.M.M., FANNING, C.M.M., VERNON, R.H.H., PATERSON, S.R.R. & TATE, M.C.C. 2003. Structure, emplacement and lateral expansion of the San José tonalite pluton, Peninsular Ranges batholith, Baja California, México. *Journal of Structural Geology*, **25**, 1933–1957, doi: 10.1016/S0191-8141(03)00015-4.

KACHI, S., MOMIYAMA, K. & SHIMIZU, S. 1963. An Electron Diffraction Study and a Theory of the Transformation from γ-Fe2O3 to α-Fe2O3. *Journal of the Physical Society of Japan*, **18**, 106–116, doi: 10.1143/JPSJ.18.106.

KINAHAN, G.H. 1869. Explanation to accompany Sheet 105 with that portion of Sheet 114 that lies north of Galway Bay. *Memoir of the Geological Survey of Ireland, Dublin*.

KINAHAN, G.H. 1878. Explanatory memoir to accompany Sheets 93 and 94, with the adjoining portions of Sheets 83, 84, and 103, of the maps of the Geological Survey of Ireland. *Memoir of the Geological Survey of Ireland, Dublin*.

KOCH, F.G., JOHNSON, A.M. & POLLARD, D.D. 1981. Monoclinal bending of strata over laccolithic intrusions. *Tectonophysics*, **74**, T21–T31, doi: http://dx.doi.org/10.1016/0040-1951(81)90189-X.

LATTARD, D., ENGELMANN, R., KONTNY, A. & SAUERZAPF, U. 2006. Curie temperatures of synthetic titanomagnetites in the Fe-Ti-O system: Effects of composition, crystal chemistry, and thermomagnetic methods. *Journal of Geophysical Research*, **111**.

LEAKE, B.E. 1969. The origin of the Connemara migmatites of the Cashel district, Connemara, Ireland. *Quarterly Journal of the Geological Society*, **125**, 219–276, doi: 10.1144/gsjgs.125.1.0219.

LEAKE, B.E. 2011. Stoping and the mechanisms of emplacement of the granites in the Western Ring Complex of the Galway granite batholith, western Ireland. *Earth and Environmental Science Transactions of the Royal Society of Edinburgh*, **102**, 1–16.

LEAKE, B.E. & LEGGO, P.J. 1963. On the Age Relations of the Connemara Migmatites and the Galway Granite, West of Ireland. *Geological Magazine*, **100**, 193–204.

LEAKE, B.E. & SINGH, D. 1986. The Delaney Dome Formation, Connemara, W. Ireland, and the Geochemical Distinction of Ortho- and Para-Quartzofeldspathic Rocks. *Mineralogical Magazine*, **50**, 205–215.

LEAKE, B.E. & TANNER, G.P.W. 1994. The Geology of the Dalradian and Associated Rocks of Connemara, Western Ireland. *Royal Irish Academy*.

LEAKE, B.E., TANNER, P.W.G., MACINTYRE, R.M. & ELIAS, E. 1984. Tectonic position of the Dalradian rocks of Connemara and its bearing on the evolution of the Midland Valley of Scotland. *Earth and Environmental Science Transactions of the Royal Society of Edinburgh*, **75**, 165–171.

LEAKE, E.B., TANNER, P.W.G., SINGH, D. & HALLIDAY, A.N. 1983. Major southward thrusting of the Dalradian rocks of Connemara, western Ireland. *Nature*, **305**, 210–213.

LISS, D., OWENS, W.H. & HUTTON, D.H.W. 2004. New palaeomagnetic results from the Whin Sill complex: evidence for a multiple intrusion event and revised virtual geomagnetic poles for the late Carboniferous for the British Isles. *Journal of the Geological Society* , **161** , 927–938, doi: 10.1144/0016-764903-156.

LOWRIE, W. 1990. Identification of ferromagnetic minerals in a rock by coercivity and unblocking temperature properties. *Geophysical Research Letters*, **17**, 159–162.

LOWRIE, W. & FULLER, M. 1971. On the Alternating Field Demagnetization Characteristics of Multidomain Thermoremanent Magnetization in Magnetite. *Journal of Geophysical Research*, **76**, 6339–6349, doi: 10.1029/JB076i026p06339.

MAGEE, C., STEVENSON, C.T.E., DRISCOLL, B.O. & PETRONIS, M.S. 2012. Local and regional controls on the lateral emplacement of the Ben Hiant Dolerite intrusion, Ardnamurchan (NW Scotland). *Journal of Structural Geology*, **39**, 66–82, doi: 10.1016/j.jsg.2012.03.005.

MARSH, B.D. 1982. On the mechanics of igneous diapirism, stoping, and zone melting. *American Journal of Science*, **282**, 808–855, doi: 10.2475/ajs.282.6.808.

MARTÍN-HERNÁNDEZ, F. & HIRT, A.M. 2001. Separation of ferrimagnetic and paramagnetic anisotropies using a high-field torsion magnetometer. *Tectonophysics*, **337**, 209–221, doi: http://dx.doi.org/10.1016/S0040-1951(01)00116-0.

MARTINS, H.C.B., SANT'OVAIA, H., ABREU, J., OLIVEIRA, M. & NORONHA, F. 2011. Emplacement of the Lavadores granite (NW Portugal): U/Pb and AMS results. *Comptes Rendus Geoscience*, **343**, 387–396, doi: http://dx.doi.org/10.1016/j.crte.2011.05.002.

MARZEC, L. 1927. Les plis diapirs et le diapirisme en general. *C.R. Seances Inst. Geol. Roumanie*, **6**, 226–270.

MCCARTHY, W. 2013. An evaluation of orogenic kinematic evolution utilizing crystalline and magnetic anisotropy in granitoids. *PhD Thesis, University College Cork, National University of Ireland*, **1**.

MILLER, C.F., WATSON, E.B. & HARRISON, T.M. 1988. Perspectives on the source, segregation and transport of granitoid magmas. *Earth and Environmental Science Transactions of the Royal Society of Edinburgh*, **79**, 135–156.

MILLER, R.B. & PATERSON, S.R. 1999. In defense of magmatic diapirs. *Journal of Structural Geology*, **21**, 1161–1173, doi: 10.1016/s0191-8141(99)00033-4.

MOLYNEUX, S.J. & HUTTON, D.H.W. 2000. Evidence for significant granite space creation by the ballooning mechanism : The example of the Ardara pluton, Ireland. *Geological Society of America Bulletin*, **112**, 1543–1558.

MORGAN, S.S., LAW, R.D. & NYMAN, M.W. 1998. Laccolith-like emplacement model for the Papoose Flat pluton based on porphyroblast-matrix analysis. *Geological Society of America Bulletin*, **110**, 96–110.

MORTON, W.H. 1964. The petrology and structure of the basic igneous complex at Roundstone, Co. Galway, Eire. *PhD Thesis, University of Manchester, UK*.

MOSKOWITZ, B.M. 1981. Methods for estimating Curie temperatures of titanomaghemites from experimentalJs-T data. *Earth and Planetary Science Letters*, **53**, 84–88, doi: http://dx.doi.org/10.1016/0012-821X(81)90028-5.

MUDGE, M.R.R. 1968. Depth Control of Some Concordant Intrusions. *Geological Society of America Bulletin*, **79**, 315–332, doi: 10.1130/0016-7606(1968)79[315:dcosci]2.0.co;2.

NELSON, C.A. & G, S.A. 1971. Wallrock decarbonation and forcible emplacement of Birch Creek pluton, southern White Mountains, California. *Geological Society of America Bulletin*, **82**, 2891–2904.

O'DRISCOLL, B., TROLL, V.R., REAVY, R.J. & TURNER, P. 2006. The Great Eucrite intrusion of Ardnamurchan, Scotland: Reevaluating the ring-dike concept. *Geology*, **34**, 189–192, doi: 10.1130/g22294.1.

O'REILLY, W. 1984. Rock and mineral magnetism. *Blackie*, 220.

ORLICKÝ, O. 1990. Detection of magnetic carriers in rocks: results of susceptibility changes in powdered rock samples induced by temperature. *Physics of the Earth and Planetary Interiors*, **63**, 66–70.

OWENS, W.H. 1974. Mathematical model studies on factors affecting the magnetic anisotropy of deformed rocks. *Tectonophysics*, **24**, 115–131, doi: 10.1016/0040-1951(74)90133-4.

OWENS, W.H. 1994. Laboratory drilling of field-orientated block samples. *Journal of Structural Geology*, **16**, 1719–1721.

OWENS, W.H. 2000a. Error estimates in the measurement of anisotropic magnetic susceptibility. *Geophysical Journal International*, **142**, 516–526, doi: 10.1046/j.1365-246x.2000.00175.x.

OWENS, W.H. 2000b. Statistical analysis of normalized and unnormalized second rank tensor data, with application to measurements of anisotropy of magnetic susceptibility. *Geophysical Research Letters*, **27**, 2985–2988, doi: 10.1029/1999gl008439.

PASSCHIER, C.W. 2005. Microtectonics. *Springer Berlin Heidelberg New York2*, **2**.

PATERSON, S.R., VERNON, R.H. & TOBISCH, O.T. 1989. A review of criteria for the identification of magmatic and tectonic foliations in granitoids. *Journal of Structural Geology*, **11**, 349–363, doi: http://dx.doi.org/10.1016/0191-8141(89)90074-6.

PATERSON, S.R., SCIENCES, E., CALIFORNIA, S. & ANGELES, L. 1995. Bursting the bubble of ballooning plutons : A return to nested diapirs emplaced by multiple processes. *Geological Society of America Bulletin*, **107**, 1356–1380.

PETFORD, N. & CLEMENS, J.D. 2000. Granites are not diapiric ! 180–184.

PETFORD, N., CRUDEN, A.R., MCCAFFREY, K.J.W. & VIGNERESSE, J.L. 2000. Granite magma formation, transport and emplacement in the Earth's crust. *Nature*, **408**, 669–673.

PETRONIS, M.S., HACKER, D.B., HOLM, D.K., GEISSMAN, J.W. & HARLAN, S.S. 2004. Magmatic flow paths and palaeomagnetism of the Miocene Stoddard Mountain laccolith, Iron Axis region, Southwestern Utah, USA. *Geological Society, London, Special Publications*, **238**, 251–283, doi: 10.1144/GSL.SP.2004.238.01.16.

PETRONIS, M.S., O'DRISCOLL, B. & LINDLINE, J. 2011. Late stage oxide growth associated with hydrothermal alteration of the Western Granite, Isle of Rum, NW Scotland. *Geochemistry, Geophysics, Geosystems*, **12**, doi: 10.1029/2010GC003246.

PETRONIS, M.S., DRISCOLL, B.O., STEVENSON, C.T.E. & REAVY, R.J. 2012. Controls on emplacement of the Caledonian Ross of Mull Granite , NW Scotland : Anisotropy of magnetic susceptibility and magmatic and regional structures. *Geological Society of America Bulletin*, 906–927, doi: 10.1130/B30362.1.

PITCHER, W.S. 1987. Granites and yet more granites forty years on. *Geologische Rundschau*, **76**, 51–79.

PITCHER, W.S. & BERGER, A.R. 1972. The Geology of Donegal. A study of granite emplacement and unroofing. *Wiley Interscience, New York*.

PITCHER, W.S. & BUSSELL, M.A. 1977. Structural control of batholithic emplacement in Peru: a review. *Journal of the Geological Society*, **133**, 249–255, doi: 10.1144/gsjgs.133.3.0249.

PITCHER, W.S.S. 1979. The nature, ascent and emplacement of granitic magmas. *Journal of the Geological Society*, **136**, 627–662, doi: 10.1144/gsjgs.136.6.0627.

POLLARD, D.D. & JOHNSON, A.M. 1973. Mechanics of growth of some laccolithic intrusions in the Henry mountains, Utah, II: Bending and failure of overburden layers and sill formation. *Tectonophysics*, **18**, 311–354, doi: http://dx.doi.org/10.1016/0040-1951(73)90051-6.

POTTER, D.K. & STEPHENSON, A. 1988. Single domain particles in rocks and magnetic fabric analysis. *Geophysical Research Letters*, **15**, 1097–1100, doi: 10.1029/GL015i010p01097.

RAMBERG, H. 1970. Model studies in relation to intrusion of plutonic bodies. *In*: *Newall, G. and Rast, N. (eds) Mechanism of Igneous Intrusion. Geological Journal Special Issue*. 261–286.

RAMSAY, J.G. 1989. Emplacement kinematics of a granite diapir: the Chindamora batholith, Zimbabwe. *Journal of Structural Geology*, **11**, 191–209, doi: 10.1016/0191-8141(89)90043-6.

RICHEY, J.E. 1927. The Structural Relations of the Mourne Granites, Northern Ireland. *Quarterly Journal of the Geological Society* , **83** , 653 – NP, doi: 10.1144/GSL.JGS.1927.083.01-05.27.

RICHTER, C. & PLUIJM, B.A. VAN DER. 1994. Separation of paramagnetic and ferrimagnetic susceptibilities using low temperature magnetic susceptibilities and comparison with high field methods. *Physics of the Earth and Planetary Interiors*, **82**, 113–123.

ROCHETTE, P. 1988. Inverse magnetic fabric in carbonate-bearing rocks. *Earth and Planetary Science Letters*, **90**, 229–237, doi: 10.1016/0012-821x(88)90103-3.

ROCHETTE, P., AUBOURG, C. & PERRIN, M. 1999. Is this magnetic fabric normal? A review and case studies in volcanic formations. *Tectonophysics*, **307**, 219–234, doi: 10.1016/s0040-1951(99)00127-4.

SNOWDEN, P.A. & SNOWDEN, D. V. 1981. Petrochemistry of the late Archean granites of thc Chindamora batholith, Zimbabwe. *Precambrian Research*, **16**, 103–129.

STEPHENSON, A. 1994. Distribution anisotropy: two simple models for magnetic lineation and foliation. *Physics of the Earth and Planetary Interiors*, **82**, 49–53, doi: 10.1016/0031-9201(94)90101-5.

STEVENSON, C.T.E. 2008. A Revised intrusion sequence for the Donegal Batholith: evidence from its aureole in Lettermacaward. *Irish Journal of Earth Sciences*, **26**, 33–43.

STEVENSON, C.T.E., HUTTON, D.H.W. & PRICE, A.R. 2006. The Trawenagh Bay Granite and a new model for the emplacement of the Donegal Batholith. *Earth and Environmental Science Transactions of the Royal Society of Edinburgh*, **97**, 455–477.

TARLING, D.H. & HROUDA, F. 1993. The Magnetic Anisotropy of Rocks Tarling, D. & Hrouda, F. (eds). *Chapman & Hall, New York*, **54**, 2429–2442.

TAUXE, L. 1998. Paleomagnetic principles and practice. *Kluwer Academic Publishers, Dordrecht*, 299.

VAUCHEZ, A., PACHECO NEVES, S. & TOMMASI, A. 1997. Transcurrent shear zones and magma emplacement in Neoproterozoic belts of Brazil. *In: Bouchez, J.L., Hutton, D.H.W., Stephens, W.E., (eds.), Grantie: From Segregation of Melt to Emplacement Fabrics, Kluwer Academic Publishers, Dordrecht*, 275–294.

VERNON, R.H. 2004. A practical guide to Rock Microstructure. *Cambridge University Press*, 43–165.

VERNON, R.H. & PATERSON, S.R. 1993. The Ardara pluton, Ireland: deflating an expanded intrusion. *Lithos*, **31**, 17–32, doi: 10.1016/0024-4937(93)90030-g.

VIGNERESSE, J.L. 2004. A new paradigm for granite generation. *Earth and Environmental Science Transactions of the Royal Society of Edinburgh*, **95**, 11–22.

VIGNERESSE, J.L. & CLEMENS, J.D. 2000. Granitic magma ascent and emplacement: neither diapirism nor neutral buoyancy. *In: Vendeville, B., Mart, Y., Vigneresse, J.L. (eds) Salt, Shale and Igneous Diapirs in and Around Europe. Geological Society London, Special Publications*, 1–19.

WEERTMAN, J. 1980. The stopping of a rising, liquid-filled crack in the Earth's crust by a freely slipping horizontal joint. *Journal of Geophysical Research: Solid Earth*, **85**, 967–976, doi: 10.1029/JB085iB02p00967.

WEINBERG, R.F. & PODLADCHIKOV, Y. 1994. Diapiric ascent of magmas through power law crust and mantle. *Journal of Geophysical Research*, **99**, 9543–9559, doi: 10.1029/93jb03461.

WOLFF, J.A., ELLWOOD, B.B. & SACHS, S.D. 1989. Anisotropy of magnetic susceptibility in welded tuffs: application to a welded-tuff dyke in the tertiary Trans-Pecos Texas volcanic province, USA. *Bulletin of Volcanology*, **51**, 299–310, doi: 10.1007/bf01073518.

XU, S. & DUNLOP, D.J. 1995. Toward a better understanding of the Lowrie-Fuller test. *Journal of Geophysical Research*, **100**, 22533–22542, doi: 10.1029/95jb02154.

YOSHINOBU, A.S., BARNES, C.G., ET AL. 2008. Is stoping a volumetrically significant pluton emplacement process?: Discussion. *Geological Society of America Bulletin*, **120**, 1080–1081, doi: 10.1130/b26141.1.

Tables

Table 1.

Parameter	T_j	P_j	H%	Km x 10^{-3}(SI)
All Sites				
Min	-0.714	1.02	3.96	1.21
Max	0.973	1.25	33.83	24.08
Mean	0.411	1.09	13.28	14.45

Std. Dev	0.347	0.05	6.81	4.13
G1				
Min	-0.334	1.03	4.19	1.207
Max	0.973	1.25	33.83	24.08
Mean	0.474	1.1	14.18	14.55
Std. Dev	0.295	0.049	6.85	4.29
G2				
Min	-0.714	1.02	3.96	9.44
Max	0.573	1.08	12.81	19.82
Mean	0.026	1.05	7.74	13.83
Std. Dev	0.388	0.016	2.56	2.95

Table 1. Summary of AMS results and determined parameters for all sample sites within the Roundstone Pluton and for each facies independently.

Figure Captions

Fig. 1. Summarised geology of the Connemara Metamorphic Complex and the late Caledonian Galway Granite Complex (GGC). The GGC constitutes the Earlier Granites (1 = Omey Pluton, 2 = Innis Pluton, 3 = Letterfrack Pluton, 4 = Roundstone Pluton) and the Main Batholith (a composite of 5 = Carna Pluton and 6 = Kilkieran Pluton). Northwest-southeast and southwest-northeast D5 faults cross the Connemara Metamorphic Complex and several intersect the Roundstone Pluton.

Fig. 2. Summary geological map of the study area (modified after Leake and Tanner (1994)) and cross section (modified after Leake (1986)). The Roundstone Pluton intrudes the Connemara Metamorphic Complex, cross cuts the host rocks WNW-ESE foliation and is cross cut by reactivated D5 faults.

Fig. 3. (a) XPL image of G1 perthitic K-feldspar with included feldspar and biotite. (b) XPL image of G2 exhibiting characteristic complexly zoned euhedral plagioclase xenocrysts. (c) Reflected light photomicrograph (G1) shows elongate magnetite grains included within, and aligned parallel to, the biotite cleavage plane and the measured K1 AMS axis. (d) Field photograph of lobate G2 contacts cross-cutting G1. (e) Pure shear inflation fabric adjacent to the pluton contact defined by quartz ribbons and smeared biotite. (f) Inner shear zone fabric defined by partially aligned K-feldspar phenocrysts, euhedral biotite and quartz ribbons.

Fig. 4 (a) Results of high temperature low field magnetic susceptibility experiments. (b) Results of cryogenic low field magnetic susceptibility experiments. (c & d) Results of IRM acquisition and back-field IRM demagnetisation. (d) Response of select samples to demagnetisation of NRM and imposed ARM and IRM. (d) Results of three component IRM thermal demagnetisation.

Fig. 5 Contour map of mean magnetic susceptibility (K_{mean}). No major fluctuation of K_{mean} is observed across facies contacts indicating a reasonably homogenous distribution of magnetite across the intrusion.

Fig. 6 (a) A contour map of Corrected Degree of Anisotorpy (P_j). The strongest H values occur in the west and east and are systematically weakest along the NNW-SSE axis of the intrusion. (b) A contour map of Shape Anisotropy (T_j). Note that the highest T_j values (highly oblate) occur along two arcs which define an oval elongate along a NNW-SSE axis and not at the pluton's margin.

Fig. 7 Results of AMS analysis with representative southern hemisphere projections of averaged AMS tensors. Each data point is plotted as a foliation, lineation or both depending on calculated anisotropy values. Stereographic projections labelled X are peripheral samples that return dominantly oblate foliations with well constrained K1 axes, labelled Y represent the inner strain zone and exhibit a girdle of K1 and K2 axes and labelled Z represent the core of the intrusion and are tri-axial or prolate.

Fig. 8 (a) Summary map of AMS and field data with interpreted structures. Fabric symbols are weighted based on T_j (symbols are smaller where T_j is closer to zero and larger when closer to -1 or +1). Prolate tensors only occur in the centre of the pluton, these are interpreted as magmatic fabrics. The strongest fabrics are oblate and occur along the inner strain zone (along dashed line). (b) Stereographic projection of AMS principal axes show a preferential orientation of K1 axes along a NNW-SSE axis and K3 axes that are concentrated in the ENE-WNW. (c) Clusters of data on a polar $P_j - T_j$ plot of AMS data are related to the pure shear flattening, internal strain and interior strain zones identified.

Fig. 9 Schematic punched laccolith model. (a) Siting of the pluton was controlled by reactivated D5 faults during regional sinistral transpression. (b) Lateral emplacement is controlled by the sub-horizontal Mannin Thrust. (c) Ductile deformation and vertical displacement of overburden facilitates lateral emplacement and laccolith inflation. (d) Tensile strength of overlying strata is exceeded, the roof is up-faulted and magma intrudes radial faults causing localised stoping of the country rock around the periphery of the intrusion.

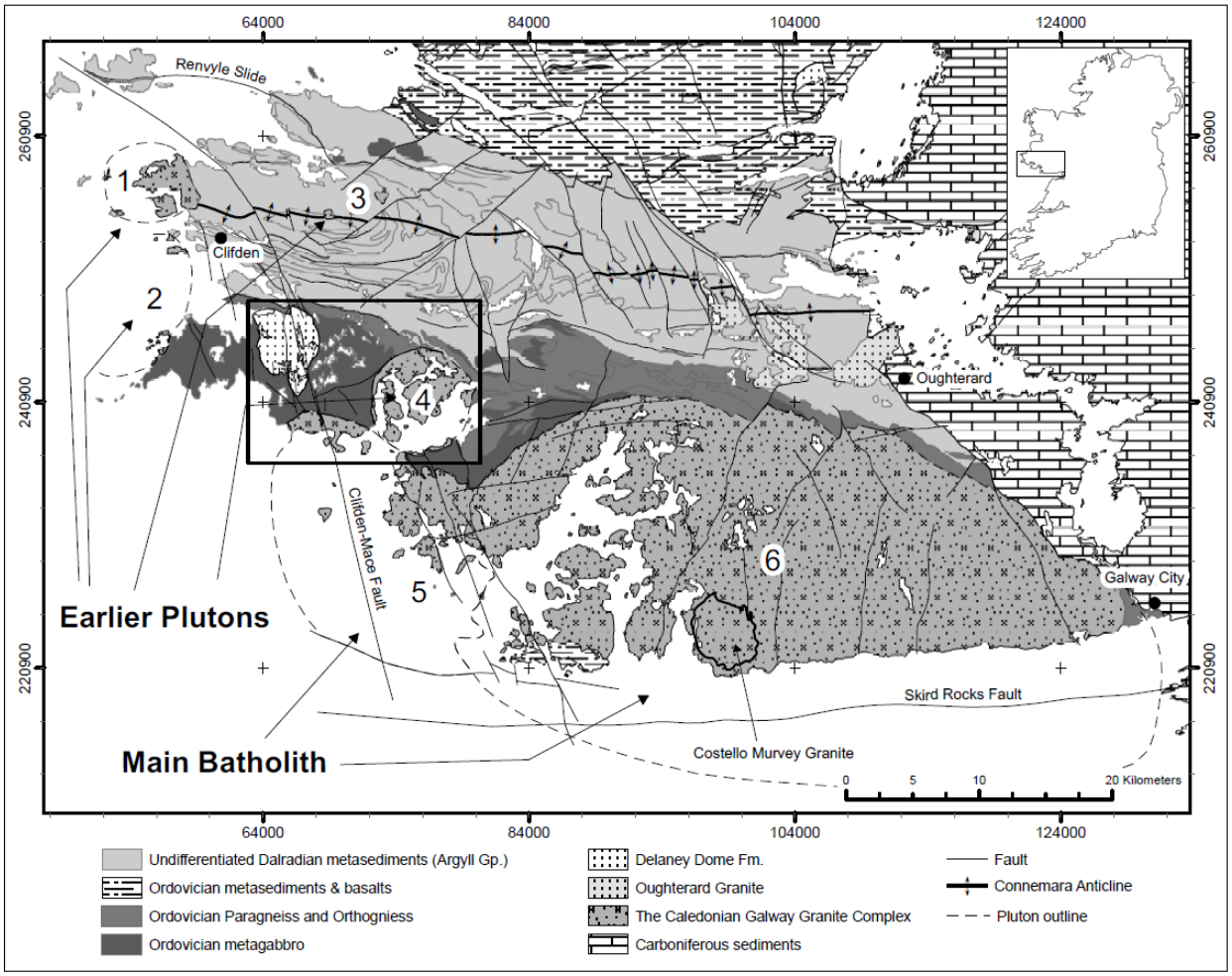
64000
84000
104000
124000
260900
240900
220900
Renvyle Slide
1
2
3
4
5
6
Clifden
Oughterard
Galway City
Clifden-Maoe Fault
Earlier Plutons
Main Batholith
Skird Rocks Fault
Costello Murvey Granite
0 5 10 20 Kilometers
Undifferentiated Dalradian metasediments (Argyll Gp.)
Ordovician metasediments & basalts
Ordovician Paragneiss and Orthogniess
Ordovician metagabbro
Delaney Dome Fm.
Oughterard Granite
The Caledonian Galway Granite Complex
Carboniferous sediments
Fault
Connemara Anticline
Pluton outline

Fig. 1

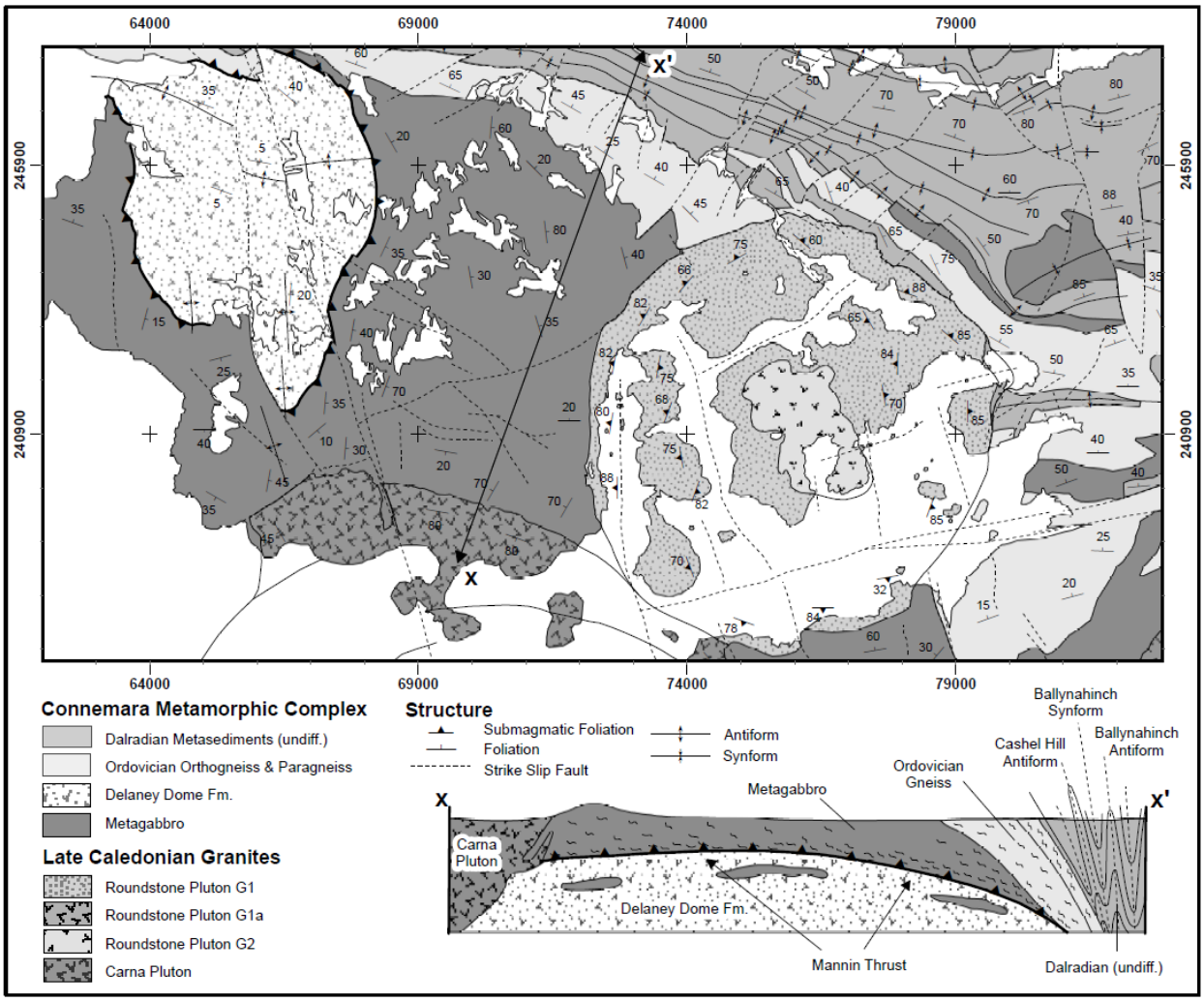
64000
69000
74000
79000
245900
240900
X
X'
Connemara Metamorphic Complex
Dalradian Metasediments (undiff.)
Ordovician Orthogneiss & Paragneiss
Delaney Dome Fm.
Metagabbro
Late Caledonian Granites
Roundstone Pluton G1
Roundstone Pluton G1a
Roundstone Pluton G2
Carna Pluton
Structure
Submagmatic Foliation
Foliation
Strike Slip Fault
Antiform
Synform
Ballynahinch Synform
Cashel Hill Antiform
Ballynahinch Antiform
Ordovician Gneiss
Metagabbro
Carna Pluton
Delaney Dome Fm.
Mannin Thrust
Dalradian (undiff.)

Fig. 2

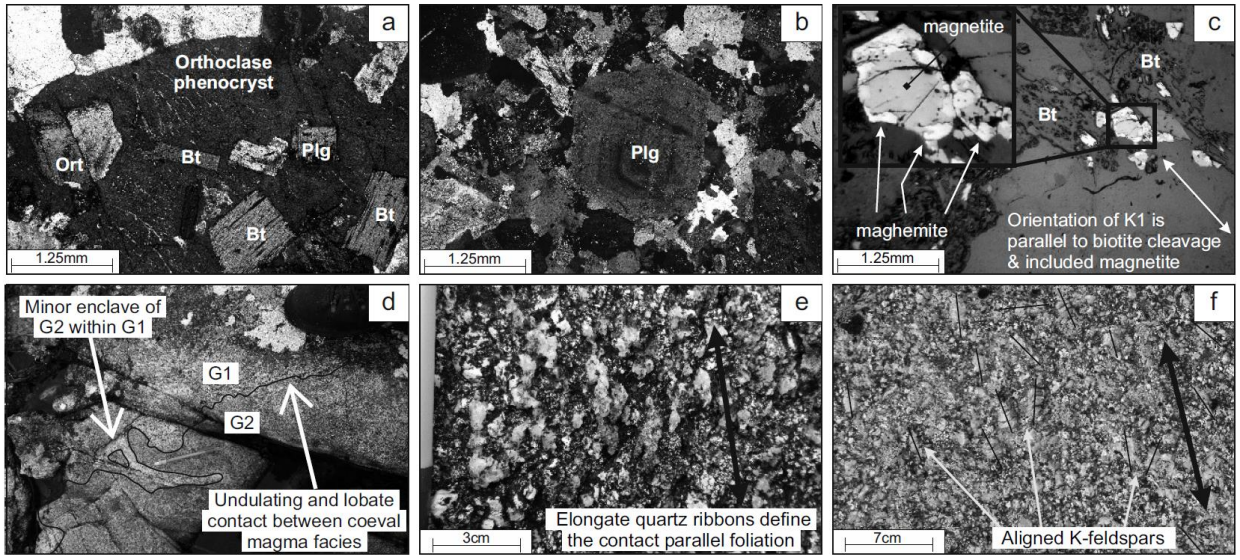

1102

1103 Fig. 3

1104

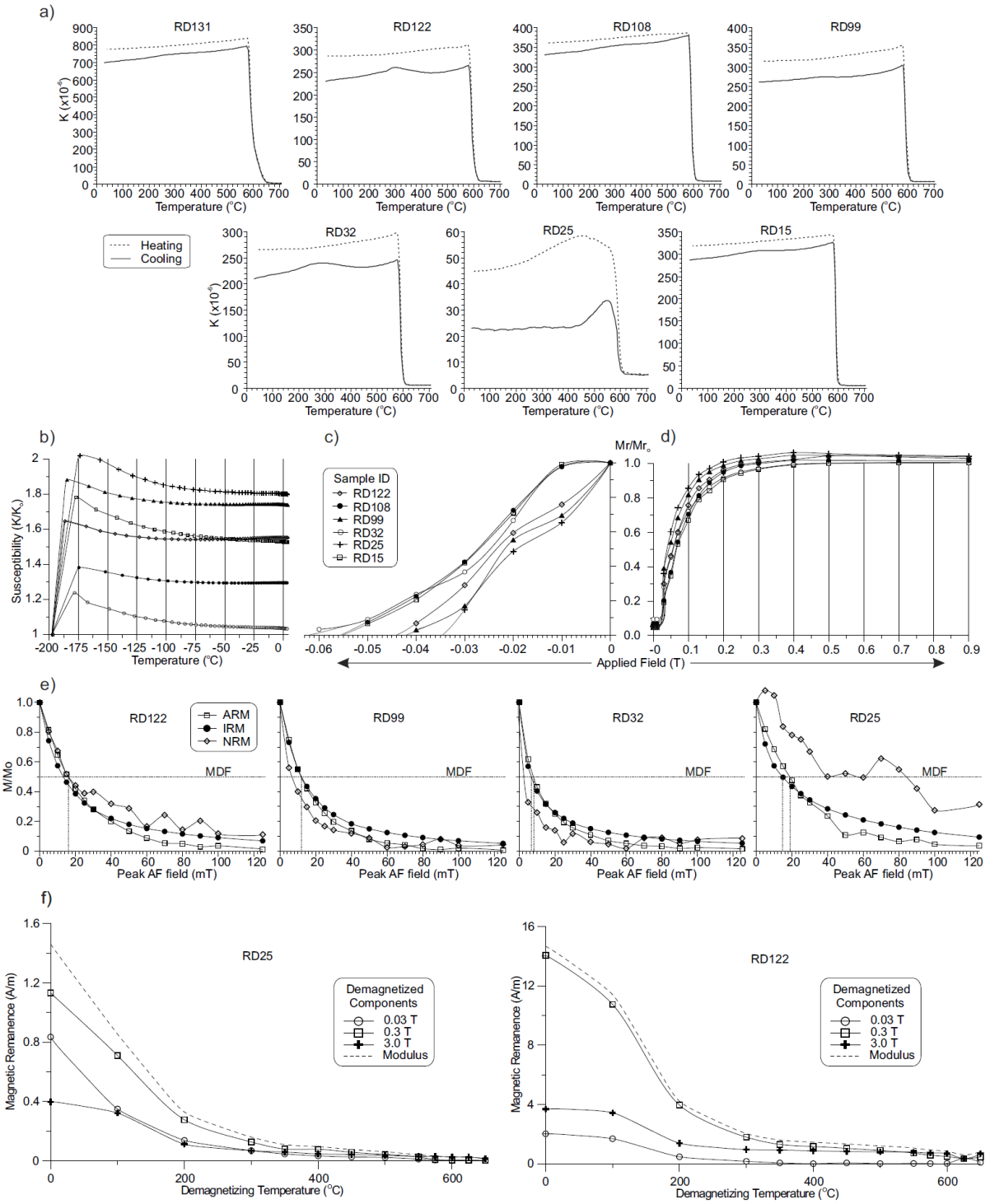
a)
RD131
RD122
RD108
RD99
RD32
RD25
RD15
K (x10⁻⁶)
Temperature (°C)
Heating
Cooling
b)
Susceptibility (K/K₀)
Temperature (°C)
c)
Sample ID
RD122
RD108
RD99
RD32
RD25
RD15
Mr/Mr₀
Applied Field (T)
d)
e)
RD122
RD99
RD32
RD25
ARM
IRM
NRM
MDF
M/Mo
Peak AF field (mT)
f)
RD25
RD122
Demagnetized Components
0.03 T
0.3 T
3.0 T
Modulus
Magnetic Remanence (A/m)
Demagnetizing Temperature (°C)

Fig. 4

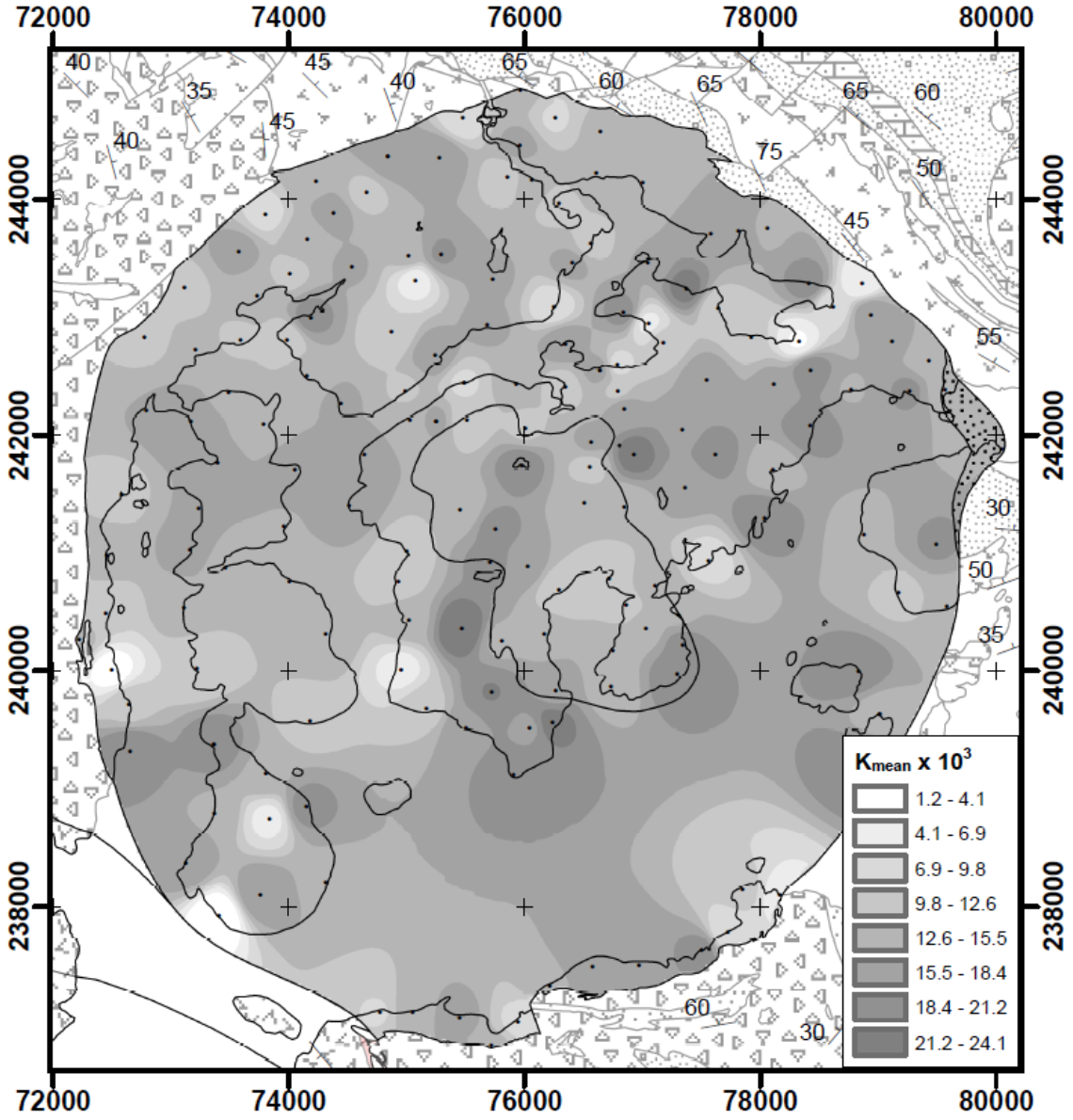

1108

1109 Fig. 5

1110

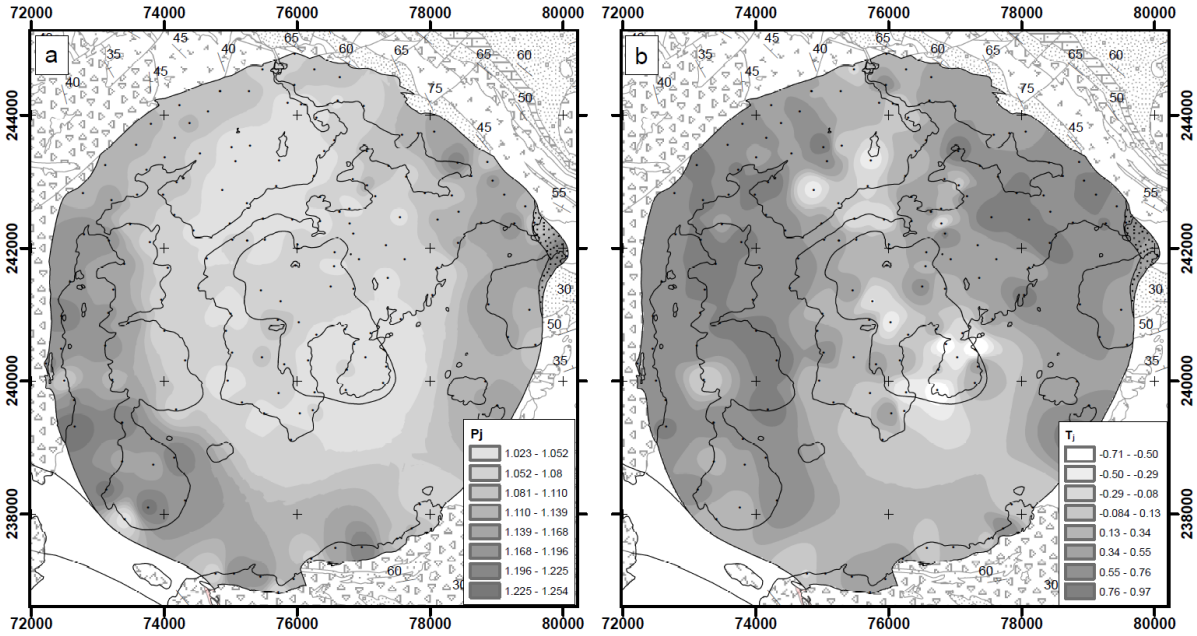
a
b
72000
74000
76000
78000
80000
244000
242000
240000
238000
Pj
1.023 - 1.052
1.052 - 1.08
1.081 - 1.110
1.110 - 1.139
1.139 - 1.168
1.168 - 1.196
1.196 - 1.225
1.225 - 1.254
Tj
-0.71 - -0.50
-0.50 - -0.29
-0.29 - -0.08
-0.084 - 0.13
0.13 - 0.34
0.34 - 0.55
0.55 - 0.76
0.76 - 0.97

Fig. 6

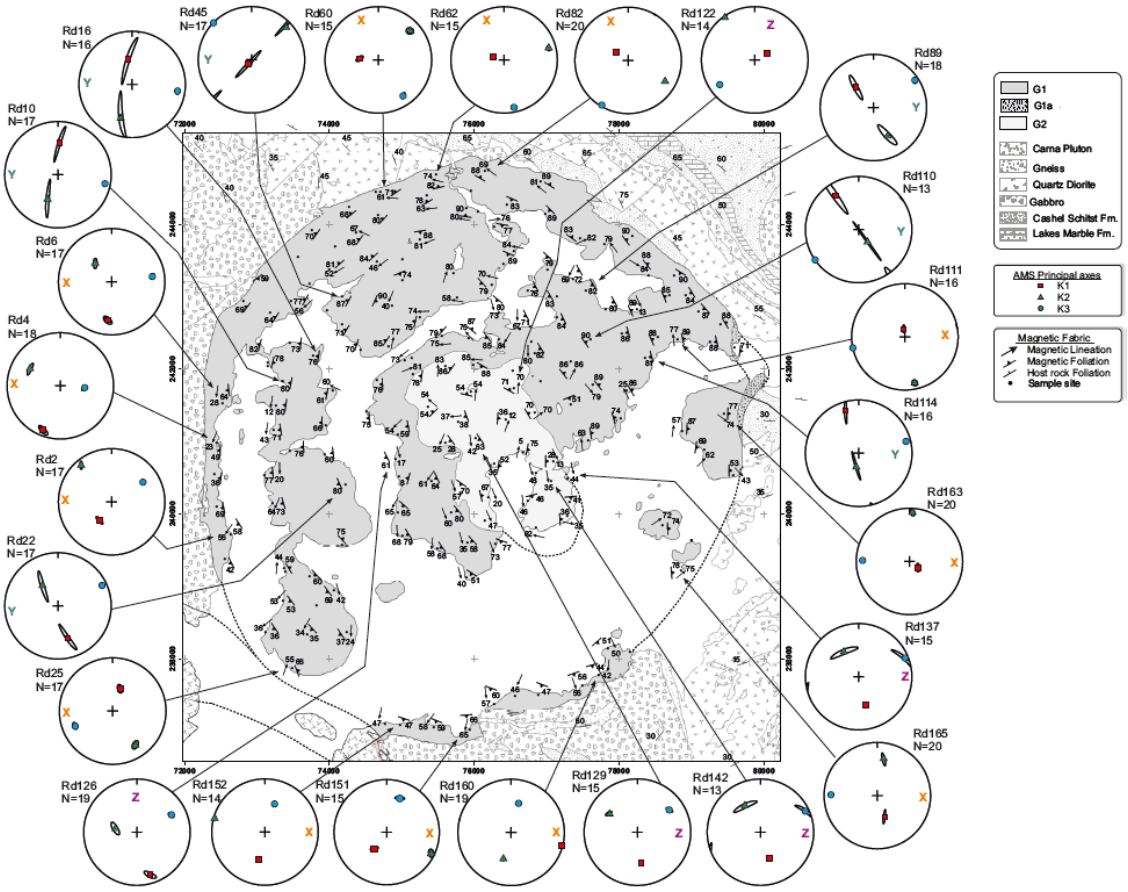
Rd45 N=17
Rd60 N=15
Rd62 N=15
Rd82 N=20
Rd122 N=14
Rd16 N=16
Rd89 N=18
Rd10 N=17
Rd110 N=13
Rd6 N=17
Rd111 N=16
Rd4 N=18
Rd114 N=16
Rd2 N=17
Rd163 N=20
Rd22 N=17
Rd137 N=15
Rd25 N=17
Rd165 N=20
Rd126 N=19
Rd152 N=14
Rd151 N=15
Rd160 N=19
Rd129 N=15
Rd142 N=13
G1
G1a
G2
Carna Pluton
Gneiss
Quartz Diorite
Gabbro
Cashel Schist Fm.
Lakes Marble Fm.
AMS Principal axes
K1
K2
K3
Magnetic Fabric
Magnetic Lineation
Magnetic Foliation
Host rock Foliation
Sample site

Fig. 7

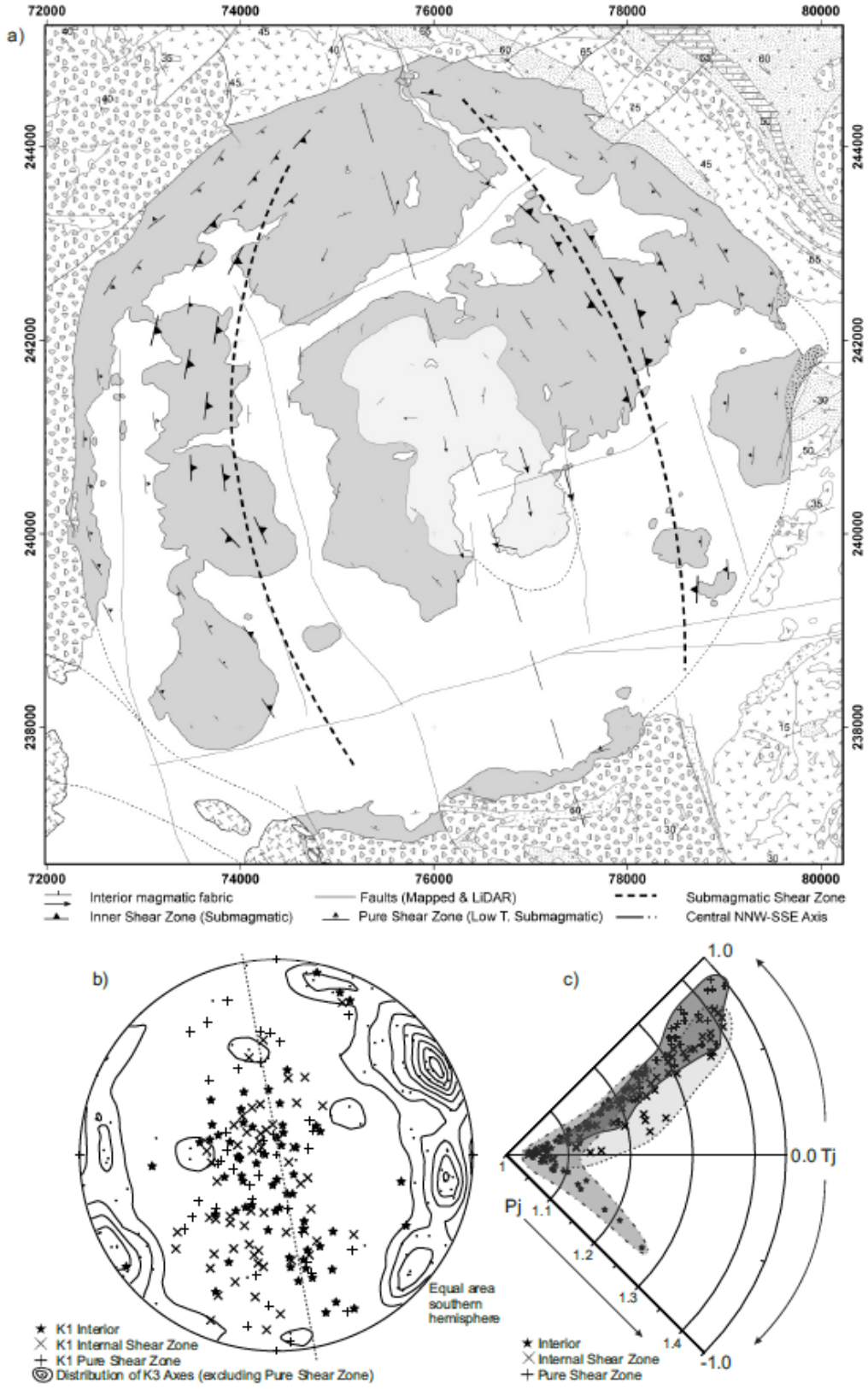

1117

1118 Fig. 8

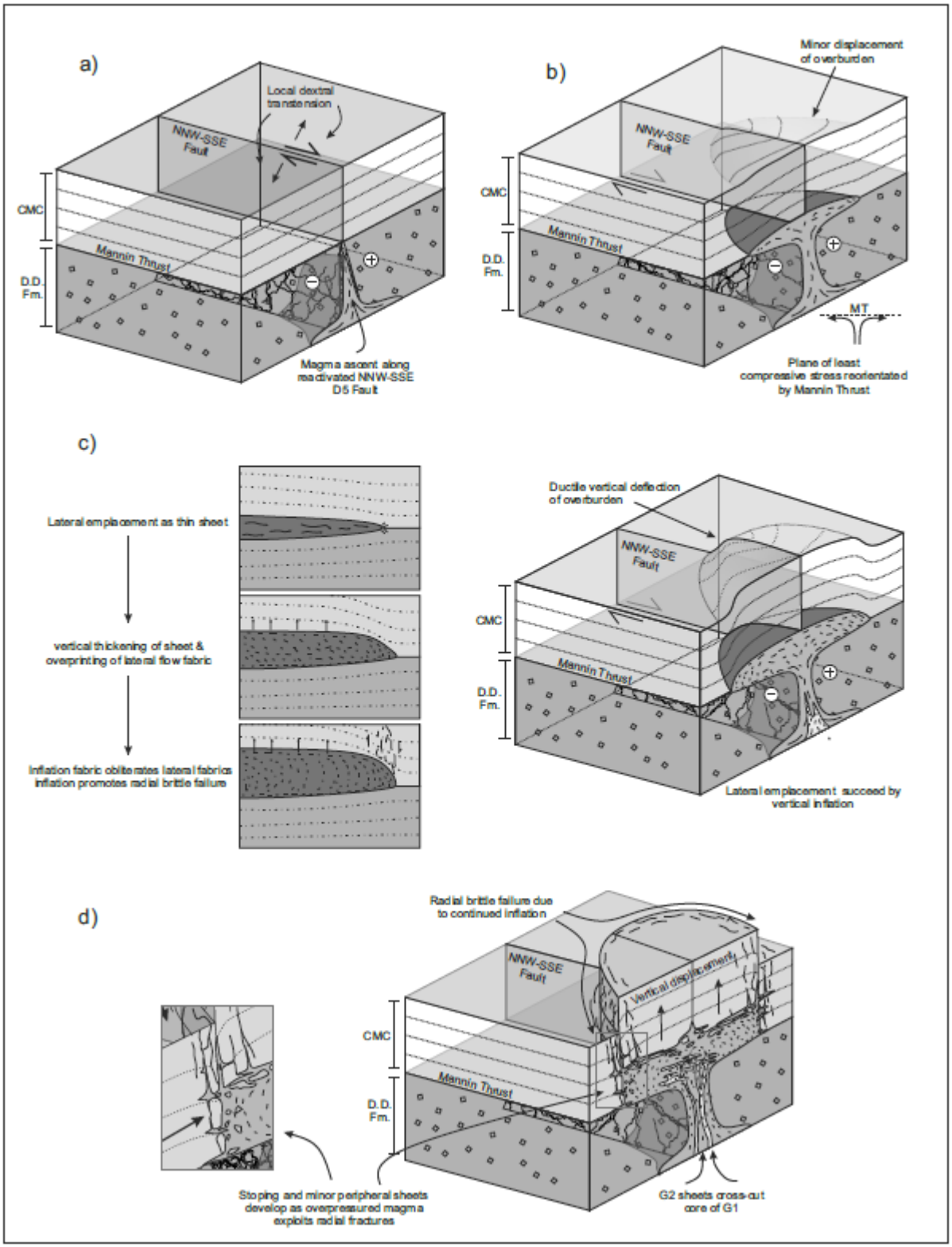

1119

1120 Fig. 9